

Canonical Latent Representations in Conditional Diffusion Models

Yitao Xu Tong Zhang Ehsan Pajouheshgar Sabine Süsstrunk
Image and Visual Representation Lab

École polytechnique fédérale de Lausanne, Lausanne, Switzerland
{yitao.xu, tong.zhang, ehsan.pajouheshgar, sabine.susstrunk}@epfl.ch

Abstract

Conditional diffusion models (CDMs) have shown impressive performance across a range of generative tasks. Their ability to model the full data distribution has opened new avenues for analysis-by-synthesis in downstream discriminative learning. However, this same modeling capacity causes CDMs to entangle the class-defining features with irrelevant context, posing challenges to extracting robust and interpretable representations. To this end, we identify *Canonical LATent Representations* (CLAREps), latent codes whose internal CDM features preserve essential categorical information while discarding non-discriminative signals. When decoded, CLAREps produce representative samples for each class, offering an interpretable and compact summary of the core class semantics with minimal irrelevant details. Exploiting CLAREps, we develop a novel diffusion-based feature distillation paradigm, *CaDistill*. While the student has full access to the training set, the CDM as teacher transfers core class knowledge only via CLAREps, which amounts to merely 10% of the training data in size. After training, the student achieves strong adversarial robustness and generalization ability, focusing more on the class signals instead of spurious background cues. Our findings suggest that CDMs can serve not just as image generators but also as compact, interpretable teachers that can drive robust representation learning.

1 Introduction

Diffusion models (DMs) excel at generative modeling of images [16, 28, 58, 65, 66]. When conditioned on class labels [4, 27, 56] or text prompts [57, 58], conditional diffusion models (CDMs) faithfully generate samples with desired characteristics of the condition. This generative capability has sparked a wave of analysis-by-synthesis approaches [5, 10, 44, 51, 53, 78, 83, 91, 95], where DMs are used to probe or improve downstream discriminative tasks. However, a key challenge remains: since DMs model the full data distribution, they often encode redundant or irrelevant information, which can obscure the discriminative signal. For example, in the *Tench* row of Figure 1, modifying the CDM latent code of the training sample changes the angler in the background while the fish remains almost unchanged, showing that the model encodes background cues that correlate with the class but not semantically essential to it. This entanglement between class semantics and extraneous factors limits interpretability and hinders the effective use of CDMs in representation learning. This motivates our central question:

How can we identify the underlying core categorical semantics in a conditional diffusion model?

We answer this by introducing Canonical LATent Representation IDENTIFIER (CLARID), a method for identifying the latent codes in CDMs that capture essential categorical information and filter out irrelevant details. We call the resulting latent codes Canonical LATent Representations (CLAREps). We begin with the assumption that the essential semantics of a class typically lie on a low-dimensional

manifold embedded in the high-dimensional data space [12, 72, 92]. We postulate that such semantic manifolds also exist within the latent space of diffusion models. Our key insight is that altering the latent code along the tangent directions of the manifold, referred to as extraneous directions, modifies visual appearance without affecting class identity. We find that projecting out the extraneous directions in the latent space of CDMs effectively eliminates class-irrelevant factors such as background clutter or co-occurring objects from other categories. When projected back to the data space, CLAReps produce representative samples of each category, namely *Canonical Samples*, providing an intuitive and interpretable summary of the essential categorical semantics. Additionally, the internal CDM features of CLAReps, *i.e.* *Canonical Features*, contain mostly the core class information. We first validate our method in a toy hierarchical generative model, where CLARID recovers a low-dimensional class manifold while standard classifier-free guidance (CFG) produces dispersed, high-likelihood samples. Scaling up, we apply CLARID to ImageNet-pretrained CDMs and develop strategies for finding the projection time step and the number of extraneous directions. Our method also generalizes to text-conditioned DMs and is compatible with different diffusion samplers.

Building on the discovery of CLARep, we propose a novel feature distillation paradigm, *CaDistill*. This method leverages the interpretable nature of CLAReps, which encapsulates the core semantics of each class, to supervise a student network. *CaDistill* aligns the student network’s representations on both Canonical Samples and original training samples with Canonical Features using a novel feature distillation loss, which helps the student network encode the core class information. The student network’s representations of the original training samples are also forced to be close to those of the Canonical Samples, treating them as anchors in the student’s representation space. The student learns on the full training set, while the teacher CDM transfers the essential class knowledge by only exploiting CLAReps, which amounts to merely 10% of the training data in size. In contrast, existing state-of-the-art methods require transferring the teacher CDM’s knowledge using the entire training set. *CaDistill* improves the student’s adversarial robustness as well as the generalization capability on CIFAR10 [40] and ImageNet [15]. Our contributions are as follows:

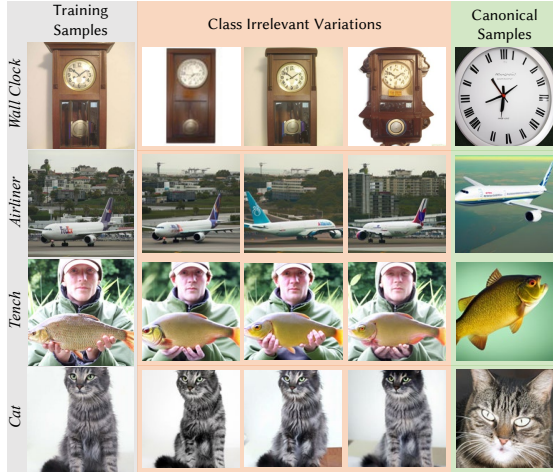


Figure 1: Conditional diffusion models (CDMs) encode both **core class features** and **irrelevant context** in a CDM. **Left**: training samples. **Middle**: samples obtained by modifying CDM latent codes that preserve the class label but alter class-irrelevant parts. **Right**: Canonical Samples produced by CLARID, which retain the **class-defining content** while removing **extraneous context**. CLARID benefits the extraction of robust and interpretable representations from the CDMs.

- We introduce *Canonical LATent Representation* (CLARep) in CDMs—latent codes whose internal CDM features, *i.e.* *Canonical Features*, encapsulate core categorical semantics with minimal irrelevant signals. When decoded to the data space, these latent codes produce *Canonical Samples*, which serve as compact and interpretable prototypes for each class.
- To extract *CLAReps*, we propose *Canonical LATent Representation Identifier* (CLARID), a method that identifies these latent codes by projecting out non-discriminative directions in the CDM’s latent space. The optimal configurations of CLARID are selected through a systematic analysis of the CDM’s features.
- Leveraging the CLAReps, we develop a novel diffusion-based feature distillation paradigm, *CaDistill*. While the student is being trained on the full training set, the CDM as the teacher transfers essential class knowledge only via exploiting CLAReps, which amounts to merely 10 % of the data. The resulting student network achieves strong adversarial robustness and generalization performance, focusing more on the core class information.

2 Related Works

2.1 Interpretability in diffusion models

Recent research in diffusion models (DMs) reveals the interpretable semantic information in them. We categorize these efforts into two main groups. The first line of this work focuses on semantic editing by manipulating the reverse diffusion trajectory to produce semantically meaningful changes in generated images [9, 22, 41, 55]. Kwon et al. [41] uncover a semantic space inside a pre-trained DM, termed h-space, where particular vector directions yield high-quality image editing results. Park et al. [55] analyze the latent input space, namely x-space, of DMs from a Riemannian geometry perspective. They define the pullback metric on x-space from the h-space Euclidean metric, obtaining certain vector directions in x-space that can yield semantic editing results. Chen et al. [9] provides more theoretical insights into this framework and extends it to local editing scenarios.

Another line of work leverages the attention mechanism [71] in DMs to interpret the conditional information [8, 26, 36, 45, 80, 94]. Hertz et al. [26] propose that the cross-attention map between the text prompts and image tokens in text-conditioned DMs encodes rich spatial cues. Building on this insight, subsequent studies analyze these attention maps to improve the precision and controllability of semantic image editing [8, 36, 45]. Other efforts investigate this property in visual recognition tasks such as semantic segmentation [80, 94], using the attention maps to interpret the model’s spatial reasoning. All existing methods either focus on image editing or are tailored to a specific DM architecture. We take the first step to uncover the underlying core class semantics in DMs without any supervision. Our method is compatible with different DM architectures and samplers.

2.2 DMs as teachers in analysis-by-synthesis

DM-based feature distillation. Recent works show that the intermediate features in DMs contain rich discriminative information [5, 10, 44, 51, 53, 78, 83, 91, 95]. Here, we focus on the utilization of DMs as teachers in feature distillation frameworks. Li et al. [44] proposes a framework in which the intermediate features of the student network are aligned to those of a generative teacher, improving the student’s performance on dense prediction tasks. Yang and Wang [83] use reinforcement learning to select a proper diffusion timestep for distillation, enhancing the student’s performance in image classification, semantic segmentation, and landmark detection benchmarks.

DMs for data generation and augmentation. DMs faithfully model the full training data distribution, which allows the generation of new training samples or augmentation of the existing ones [2, 3, 20, 21, 24, 29, 61, 63, 64, 70, 73]. Goyal et al. [21] and Schwag et al. [63] improve the robustness of adversarially-trained classifiers by using diffusion-generated data. Bansal and Grover [3] demonstrate that supplementing training data with diffusion-generated images leads to consistent gains on out-of-distribution test sets. Diffusion-generated data is also effective in data-scarce settings, *i.e.*, zero-shot and few-shot learning [20, 24, 70]. Regarding data augmentation, Islam et al. [29] propose blending images while preserving their labels using pre-trained text-to-image DMs [58]. Shama Sastry et al. [64] utilize denoised samples for augmenting the training data, improving the generalization of downstream classifiers.

Despite the progress, current methods use raw diffusion features and outputs, which contain class-irrelevant information. Such irrelevant signals prevent the student from efficiently and accurately learning the class semantics, leading to vulnerable models. On the contrary, our method transfers the core class semantics using CLAReps to the student, enhancing its adversarial robustness and generalization capability. Notably, CLAReps amounts to only 10% of the original data in size.

3 Method

An overview of Canonical Latent Representation Identifier (CLARID) is shown in Figure 2. We describe the procedure of finding the CLARep of a given sample in Section 3.2. We then provide the intuition of the effect of CLARID in a proof-of-concept experiment in Section 3.3.

3.1 Preliminaries

Diffusion models (DMs) generate images by learning to reverse a fixed forward diffusion process [28]. Let \mathbf{x}_0 be a training sample and $t \in \{1, \dots, T\}$ denote the diffusion time steps. A forward kernel $q(\mathbf{x}_t | \mathbf{x}_{t-1})$ progressively corrupts \mathbf{x}_0 into a noisy sample \mathbf{x}_t . A neural network $\mathbf{f}_{\theta,t}(\mathbf{x}_t)$, parameterized by θ , is trained to approximate the reverse process $p_{\theta}(\mathbf{x}_{t-1} | \mathbf{x}_t)$. More details are

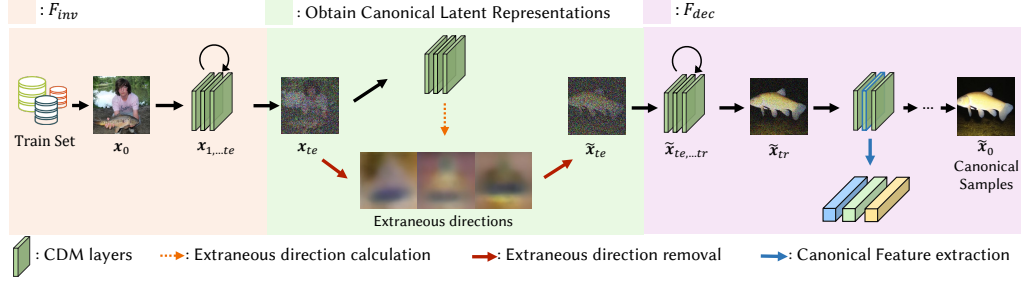


Figure 2: Overview of Canonical Latent Representation Identifier (CLARID). Starting from a training sample x_0 , we invert it using a CDM until $t = t_e$. We compute the extraneous directions using the method described in Section 3.2, and remove them from the inverted sample x_{te} to obtain a CLARep \tilde{x}_{te} . We then generate the Canonical Sample \tilde{x}_0 and extract the Canonical Feature at timestep $t = t_r$. The CDM receives the ground truth condition of x_0 in the whole process, here the *Tench* class.

in Section B in the Appendix. Certain parameterizations of the diffusion process [31, 33, 65] allow for partial or full inversion of a given input sample, producing a noisy sample x_t that preserves the semantic information of x_0 [97]. Hereafter, we denote the inversion process of a sample by F_{inv} and the corresponding decoding process as F_{dec} .

3.2 The overall procedure of Canonical Latent Representation Identifier (CLARID)

Given a sample x_0 as the seed, which belongs to class condition c , we first invert it to timestep t_e via F_{inv} . Denote x_{te} as the latent code of x_0 at t_e . In this latent space, we identify a set of extraneous directions that preserve class identity yet induce large changes. Concretely, let $f_{\theta}^l(\cdot)$ be the CDM’s feature extractor at layer l and timestep t_e . A first-order Taylor expansion around x_{te} gives:

$$f_{\theta,te}^l(x_{te} + v) \approx f_{\theta,te}^l(x_{te}) + \nabla f_{\theta,te}^l(x_{te}) \cdot v = f_{\theta,te}^l(x_{te}) + J_{\theta,te}^l(x_{te}) \cdot v. \quad (1)$$

$J_{\theta,te}^l(x_{te})$ denotes the Jacobian of $f_{\theta,te}^l(x_{te})$. Hereafter, we drop θ and l to avoid clutter. A vector v that can cause large changes in the output carries some semantic information [55, 67], but such information is **not necessarily class-relevant**, as shown in Figure 1. The change caused by vector v is defined as the L2-norm of the Jacobian vector product: $\|J_{te}(x_{te}) \cdot v\|_2$. Accordingly, the directions that lead to large changes in the output are the right singular vectors of J_{te} . When f receives conditional information c , those directions will **preserve the class identity** while altering the appearance of the decoded sample. We show examples in Section D in the Appendix. We therefore remove the components of x_{te} along those extraneous directions to obtain CLARep \tilde{x}_{te} , by projecting x_{te} onto the subspace which is orthogonal to these directions, as described in Eq.2.

$$\tilde{x}_{te} := x_{te, \perp V_k} = (\mathbf{I} - \mathbf{V}_k \mathbf{V}_k^T) x_{te}. \quad (2)$$

Here, $\mathbf{V} = [v_1, v_2, \dots]$ is the right singular vector matrix of J_{te} , and k denotes the number of singular vectors to be removed. We then apply F_{dec} to \tilde{x}_{te} to obtain one Canonical Sample \tilde{x}_0 for the input condition c . Note that the CDM is conditioned on c in the whole procedure. Additional discussion on the choice of the layer index l for computing J_{te} is provided in Section E of the Appendix.

3.2.1 Finding the optimal t_e and k

Choosing an appropriate t_e is critical for CLARID to be effective. If t_e is too small, *e.g.*, $t_e \approx \frac{T}{100}$, the synthesized sample barely changes and remains close to the original input. On the other hand, when t_e is too large, the conditional signal becomes ineffective and fails to guide the generation [42, 93]. To find the largest time step where the conditional signal is still able to steer the CDM’s output toward the desired class, we perform a two-stage sampling process starting from $p(x_T) \sim \mathcal{N}(\mathbf{0}, \mathbf{I})$:

1. **Unconditional stage** ($T \leq t < t_e$): Forward the model without class conditioning, *i.e.*, $c = \emptyset$.
2. **Conditional stage** ($t_e \leq t \leq 0$): The class condition is introduced and retained down to $t = 0$.

We generate m samples for each condition in a given dataset, and measure the accuracy of pre-trained classifiers on the generated samples. We find the saturation point of the accuracy curve as the appropriate t_e . We show the accuracy curve and more details for an ImageNet 256 \times 256-pretrained DiT [56] and a Stable Diffusion model [58] in Section H.1 in the Appendix.

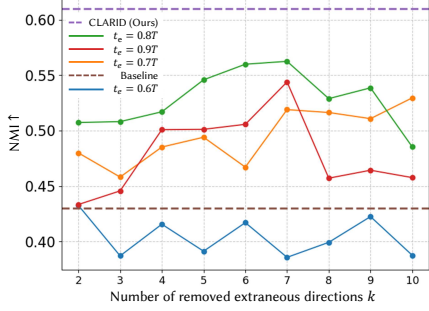


Figure 3: The normalized mutual information (NMI, higher is better) between cluster assignments of CDM features and the ground truth labels. CLARID achieves the highest NMI. Baseline is the original CDM features.

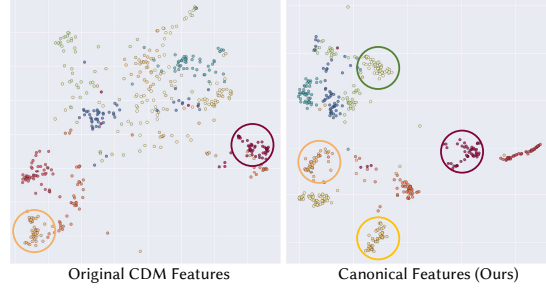


Figure 4: A 2D UMAP [50] projection of the CDM feature space, showing clusters for ten classes. Colors indicate classes. CLARID yields more compact feature clusters than the original samples (green, yellow) and preserve the existing ones (red, orange).

We fix the inversion time step t_e across all samples, but the number of directions to discard should be adapted to each sample. To decide k , we examine how strongly the top- k extraneous directions alter the sample’s visual appearance, quantified by the explained variance ratio (EVR) $S_k = \sum_{i=1}^k \sigma_i^2 / \sum_{j=1}^n \sigma_j^2$, where σ_i is the i th singular value of J_{t_e} and n is a hyperparameter. Intuitively, the extraneous direction that leads to larger variations carries less core class semantics. We compute a sequence of the EVR S_1, S_2, \dots, S_n and set the elbow point of the sequence to be the optimal k for a given sample. Compared to a fixed k , the adaptive choice will find the point where the effect of the extraneous directions diminishes. Visual examples illustrating the necessity of adapting k for each sample, along with details of deciding n and the calculation of the elbow point, are provided in Section H.2 in the Appendix.

Empirical validation. To demonstrate the effectiveness of our strategies on finding t_e and k , we quantify the feature quality of a CDM and show that our strategies achieve the best one. We also provide visual comparisons in Figure 21, 22 in the Appendix. Intuitively, by retaining the essential class features with minimal class-irrelevant information, the CDM features associated with the CLAReps (Canonical Features) should be more easily separable in the feature space. To show this, we first perform K-means clustering on the CDM features of 1000 samples from 20 different ImageNet classes (details in Section G in the Appendix), as well as their corresponding Canonical Features. We then quantify the feature quality using normalized mutual information (NMI) between the cluster assignments and the ground truth class labels. This method is training-free, hence efficient. Section G in the Appendix provides evidence on the validity of our feature quality quantification method. We perform the analysis on an ImageNet 256×256 -pretrained DiT-XL model [56]. The result is shown in Figure 3. Removing different numbers of extraneous directions, *i.e.*, varying k , yields different NMI scores, whereas CLARID adaptively chooses k for each sample and achieves the highest NMI. Qualitatively, CLARID produces feature clusters that are more compact than those formed by the original samples while preserving the existing clusters, as shown in Figure 4. We refer the readers to Section G.1 in the Appendix for the details of the feature extraction setup, including both the network layer and its associated time step t_r .

3.3 A proof-of-concept experiment

We demonstrate the effect of CLARID with a simple yet illustrative example. Figure 5a shows samples generated from our toy generative process and the corresponding density map. The process first generates class-specific samples on a segment $L = \{(x_1, 0) | 4y - 0.1 \leq x_1 \leq 4y + 0.1\}$, where $y \in \{0, 1\}$ denotes the class labels. It then adds class-independent noise to the points to generate the observed data. The samples from class 0 are included solely to introduce an inter-class contrast. We train a small class-conditional diffusion model on this data. After training, we perform CLARID on randomly selected samples from class 1. As a baseline, we take the latent codes obtained with F_{inv} and perform classifier-free guidance (CFG), steering the generation process toward regions with higher class-1 likelihood. The results are shown in Figure 5. Notably, CLARID pushes most samples to a 1D manifold inside class 1, whereas CFG mainly steers the samples away from class 0. This low-dimensional manifold described by Canonical Samples can be regarded as a summarization of class 1 information in this case. The underlying structure revealed by Canonical Samples corresponds to one of the true generative processes for the observed data, which is the one used in our toy model.

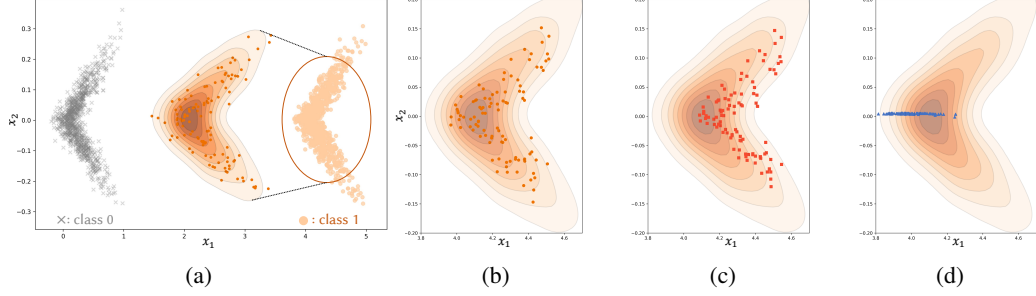


Figure 5: A toy example of CLARID. (a): The samples of **class 0** and **class 1**; (b,c,d): The generated class-1 samples of (b): **Plain F_{dec}** , (c): **CFG**, and (d): **CLARID**, respectively, after applying F_{inv} to the samples. CLARID produces Canonical Samples that lie on a 1D manifold inside class 1, offering an intuitive visual summary of the core class semantics.

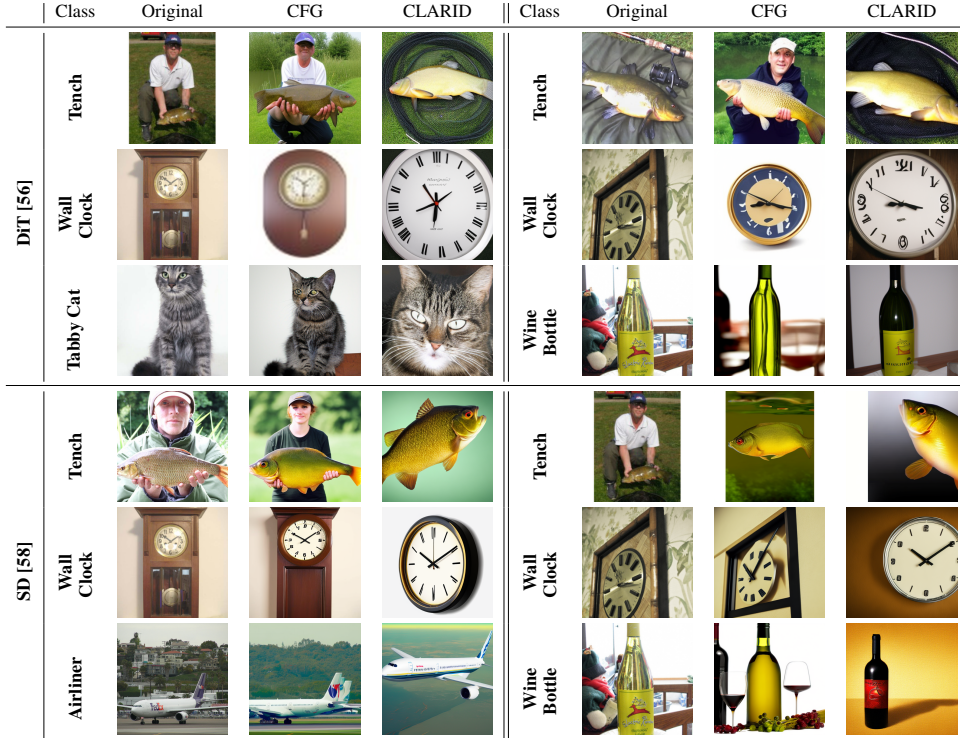


Figure 6: Comparison of classifier-free guidance (CFG) and CLARID on an ImageNet 256×256 DiT [56] and Stable Diffusion 2.1 (SD) [58]. We use the following prompt template for SD: *a photo of <Class>* [43]. CLARID focuses on identifying CLAREps to preserve the core class information, yielding Canonical Samples that provide an interpretable summary of the essential class semantics, whereas CFG aims at finding high-likelihood images. Two Canonical Samples from the *Tench* and *Wall Clock* class are presented to show that CLAREps do not collapse to a single constant vector. All "Original" images are taken from ImageNet. More visual results are in Section N in the Appendix.

We refer readers to Section I in the Appendix for details of the toy experiments. Reliably recovering the exact generative model is intractable due to the identifiability issue [48]. The solution generally requires extra inductive bias in modeling data distribution, which we leave for future work.

3.4 Qualitative results

Scaling up, we demonstrate the qualitative effect of CLARID for two pre-trained CDMs, a class-conditioned DiT [56] trained on the ImageNet 256×256 dataset and a Stable Diffusion 2.1 model [58] trained on a subset of LAION-5B [62]. We use DDIM [65] as the sampler and use 100 diffusion steps for both generation and inversion. Visual results are shown in Figure 6. We adopt classifier-free guidance after removing extraneous directions in CLARID to ensure the data fidelity, and compare

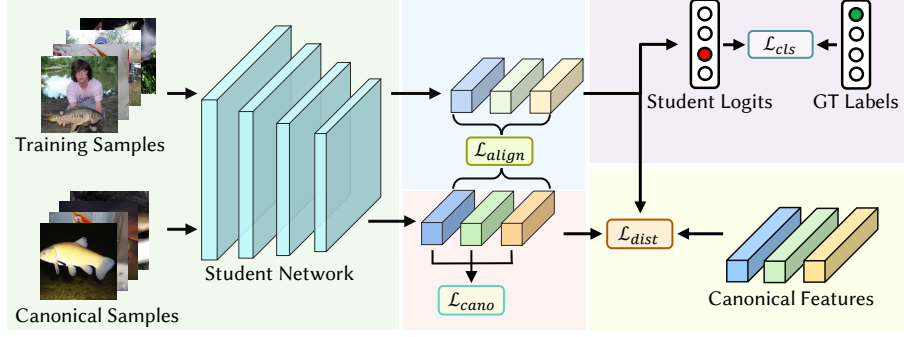


Figure 7: Overview of **CaDistill**. We align the student’s features of training images to those of Canonical Samples using \mathcal{L}_{align} . The student is trained to discriminate between Canonical Samples in different classes by optimizing \mathcal{L}_{cano} . The CDM, as a teacher, provides Canonical Features for feature distillation with \mathcal{L}_{dist} . Finally, the student is supervised on the ground-truth labels via \mathcal{L}_{cls} .

the results against pure CFG. The CLAREps visualized as Canonical Samples show that our method preserves the core class information in the original images, while CFG focuses on increasing the class-conditional likelihood. We provide more visual results in Section N in the Appendix. Occasionally, CLARID can select suboptimal t_e and k , leading to artefacts in the generated images. The failure cases are shown in Figure 29, 30 in the Appendix.

3.5 On the generalization of CLARID

While we focus on class-conditional DMs to develop the CLARID framework, it also extends naturally to text-conditioned models *e.g.* Stable Diffusion [58], as shown in Figure 6 and Section F in the Appendix. Text prompts span a far richer semantic space than one-hot class labels, giving finer control over where the CLAREps lie. We show examples of the effect using different prompts on the same input in Section F.1 in the Appendix. Understanding how this semantic structure shapes the located CLAREps is an interesting direction to explore. CLARID is also compatible with different DM samplers, as shown in Section F.2 in the Appendix.

4 The application of CLAREps

As demonstrated in Section 3, CLAREps correspond to the essential class information learned by the CDMs. Building on this insight, we design a feature distillation framework for CLAREps, termed **CaDistill**, as illustrated in Figure 7. Given a training batch $B = \{(x_1, c_1), (x_2, c_2), \dots, (x_b, c_b)\}$ where x_i is an image and c is the class label, we first **randomly** select a CLAREp \tilde{x}_i corresponding to the category of each sample. The random sampling relaxes the constraint of the size equivalence between the training dataset and the set of CLAREps. Let $P_i = \{j \in \{1, 2, \dots, b\} \mid c_j = c_i\}$ be the set of indices of samples in the batch with class label c_i . We then compute student features $z_i = g_\phi(x_i) \in \mathbb{R}^d$, $\tilde{z}_i = g_\phi(\tilde{x}_i) \in \mathbb{R}^d$, where g denotes the student network and ϕ is the set of its training parameters. The first component in **CaDistill**, \mathcal{L}_{align} , is designed to pull each training image feature towards all same-class Canonical Samples, and push away the ones from other classes. It is given in Eq. 3.

$$\mathcal{L}_{align} = -\frac{1}{b} \sum_{i=1}^b \frac{1}{|P_i|} \sum_{j \in P_i} \log \frac{\exp(z_i \cdot \tilde{z}_j / \tau)}{\sum_{k=1}^B \exp(z_i \cdot \tilde{z}_k / \tau)}. \quad (3)$$

τ is a temperature hyperparameter. Second, we encourage all Canonical Samples of the same class to cluster in the student’s feature space, and separate those of different classes. It is achieved by minimizing \mathcal{L}_{cano} in Eq. 4. When a Canonical Sample has no same-class positives, we simply optimize the denominator. See Section K.7.5 in the Appendix for more details.

$$\mathcal{L}_{cano} = -\frac{1}{b} \sum_{i=1}^b \frac{1}{|P_i| - 1} \sum_{j \in P_i, j \neq i} \log \frac{\exp(\tilde{z}_i \cdot \tilde{z}_j / \tau)}{\sum_{k \neq i} \exp(\tilde{z}_i \cdot \tilde{z}_k / \tau)}. \quad (4)$$

We perform an ablation study on the design of \mathcal{L}_{cano} by replacing it with a classification loss on the Canonical Samples in Section K.7.5 in the Appendix, demonstrating the advantage of the current \mathcal{L}_{cano} . For feature distillation, we transfer the structures of Canonical Features to the student via

Table 1: Quantitative comparisons of **CaDistill** and baselines on CIFAR-10 [40] (ResNet-18) and ImageNet [15] (ResNet-50). \mathcal{D} : Dataset. Adversarial robustness benchmarks: PGD [49], CW [7], APGD-DLR / APGD-CE [13]; Evaluations of generalization ability : Corruption (CIFAR10-C and ImageNet-C) [25], ImageNet-A [17], ImageNet-ReaL [6]. Data_{DM} is the portion of data for which the DM acts as teacher. Higher is better. Values lower than the vanilla model are in red. \dagger : the model relies on unconditional DMs, or the training cannot be performed, see Section K.6 in the Appendix.

\mathcal{D}	Model	Data_{DM}	Clean	PGD	CW	APGD-DLR	APGD-CE	Corruption	IM-A	IM-ReaL
CIFAR10	Vanilla	/	92.4	33.4	20.9	34.2	32.0	76.1	–	–
	SupCon [34]	/	92.7	29.1	16.8	34.8	29.9	76.9	–	–
	RepFusion † [83]	100%	92.7	30.3	17.2	32.1	29.2	75.3	–	–
	DMDistill	100%	92.9	41.3	32.8	38.7	36.0	76.7	–	–
	CFGDistill	10%	92.9	43.7	37.3	40.9	39.0	76.6	–	–
	CaDistill	10%	93.1	47.9	43.1	44.1	43.3	77.7	–	–
ImageNet	Vanilla	/	75.9	15.6	13.7	17.2	16.7	45.9	6.3	82.8
	DiffAug [64]	100%	76.0	15.9	13.1	17.2	17.0	47.2	4.8	83.1
	DMDistill	100%	75.7	15.7	14.1	17.0	16.7	43.6	5.0	82.8
	CFGDistill	10%	75.7	20.8	20.3	20.8	21.4	45.6	6.0	82.7
	CaDistill	10%	75.9	21.9	21.7	22.5	22.3	46.1	6.7	83.1

minimizing $\mathcal{L}_{\text{dist}}$. Specifically, we use the Centered Kernel Alignment (CKA) [39] metric to align the student’s representations of both the training images and the Canonical Samples with the Canonical Features extracted from the CDM. Maximizing CKA, *i.e.* minimizing $\mathcal{L}_{\text{dist}}$, aligns the linear subspace spanned by the student’s feature vectors with that of the teacher, effectively distilling the teacher’s class-discriminative structure into the student. Denote the student feature matrices of training images and Canonical Samples as $\mathbf{Z} \in \mathbb{R}^{b \times d}$ and $\tilde{\mathbf{Z}} \in \mathbb{R}^{b \times d}$, respectively, and the Canonical Feature matrix as $\mathcal{A} \in \mathbb{R}^{b \times d'}$. The Canonical Features are extracted from a frozen CDM for all \tilde{x}_i in a training batch.

$$\mathcal{L}_{\text{dist}} = \lambda_{cka} \log(1 - \text{CKA}(\mathbf{Z}, \mathcal{A})) + (1 - \lambda_{cka}) \log(1 - \text{CKA}(\tilde{\mathbf{Z}}, \mathcal{A})). \quad (5)$$

We find that using CKA for structural alignment outperforms existing diffusion-based feature distillation methods [44, 54, 59, 83] and refer the readers to Section K.1 in the Appendix for more details. Finally, the student is trained with the standard cross-entropy loss \mathcal{L}_{cls} on ground-truth labels. The final loss function for **CaDistill** is given in Eq. 6.

$$\mathcal{L}_{\text{CaDistill}} = \mathcal{L}_{\text{cls}} + \lambda_{cs}(\lambda_{cf}\mathcal{L}_{\text{align}} + (1 - \lambda_{cf})\mathcal{L}_{\text{cano}}) + \lambda_{\text{dist}}\mathcal{L}_{\text{dist}} \quad (6)$$

4.1 CLAREps in practice

We conduct experiments of **CaDistill** on CIFAR10 [40] using a pre-trained UNet-based CDM [28, 78] and on ImageNet using the ImageNet 256×256 -trained Diffusion Transformer (DiT) [56]. We choose two different DM architectures to demonstrate the applicability of our method. The CDM on CIFAR10 does not have an unconditional branch. The DMs are trained on the same dataset as the student models, hence no extra data is considered [64]. We follow this principle to choose the baselines, comparing our method with the SOTA diffusion-based feature distillation [83] and data augmentation [64] methods. In addition, we design two important baselines. The first one, DMDistill, is to distill the raw space structure in CDMs using $\mathcal{L}_{\text{dist}}$ on all training samples, which represents the current mainstream idea of using DMs as teachers in feature distillation. It outperforms existing diffusion-based feature distillation losses [44, 54, 59, 83] (Section K.1 in the Appendix). Second, for the CFGDistill baseline, we train the student model using the same framework of **CaDistill**, except that the images and features are obtained using CFG. For the CDM on CIFAR10, we sample new images for CFGDistill as this CDM lacks the unconditional branch and cannot perform CFG. We fix t_r , *i.e.* the feature extraction time step, for all methods that do not adaptively change it [83]. For the student network, we use ResNet18 [23] on CIFAR10 and ResNet50 [23] on ImageNet, two well-established convolutional neural network baselines [83]. We conduct PGD [49], CW [7], APGD-DLR [13], and APGD-CE [13] attacks to test the adversarial robustness of the student. On CIFAR10, we report the Top-1 accuracy on the CIFAR10-C dataset [25] as the metric for evaluating generalization. On ImageNet, we show the Top-1 accuracy on ImageNet-C (IM-C) [25], ImageNet-A (IM-A) [17], and ImageNet-ReaL (IM-ReaL) [6]. We refer readers to Section J in the Appendix for more training and evaluation procedure details.

The results are shown in Table 1. ***CaDistill*** consistently improves the adversarial robustness and generalization ability of the student, while the main effect of SOTA methods is improving the clean accuracy or a single aspect of the robustness. A more detailed discussion of the results, including the difference between CIFAR10 and ImageNet, is in Section L in the Appendix. Moreover, we consider an interesting and challenging baseline that is capable of extracting class semantics, *i.e.*, using the class token in an ImageNet-pretrained ViT [68, 69] as the teacher. We show the results in Section K.4 in the Appendix. ***CaDistill*** is effective when the student has transformer-based vision backbones, as shown in Section K.8 in the Appendix.

The student, trained with ***CaDistill***, focuses more on the core class signal. We demonstrate this by a test on the Backgrounds Challenge [79], where the background of an image that is irrelevant to the class identity is either removed or shuffled. We provide visualization of the images in Section K.5 in the Appendix. The results are given in Table 2. ***CaDistill*** improves the student performance on BG-Rand and Only-FG while maintaining the accuracy on the Original and BG-Same splits, indicating a mitigation in the model’s dependence on the spurious background cues for classification. A more detailed discussion of the results is in Section K.5 in the Appendix.

Ablation studies. Section K.7 include the ablation analysis on ***CaDistill***, including:

- **Number of CLAReps.** We demonstrate that 10% of CLAReps is sufficient for achieving competitive performance, implying the low-dimensionality property of the class manifolds in CDMs.
- **Necessity of \mathcal{L}_{align} , \mathcal{L}_{cano} , \mathcal{L}_{dist} , and their balance.** We empirically conclude the effects of all loss functions and choose the optimal weighting schemes, including λ_{cs} , λ_{cf} , λ_{dist} , λ_{cka} .
- **CFG magnitude.** We perform CFG after obtaining CLAReps, and show a proper choice of its magnitude. Importantly, a higher CFG magnitude does not contribute to better performance, indicating that ***CaDistill*** is not merely providing a converging prior on the student features. We also provide a discussion on this topic in Section G.2 in the Appendix.

5 Limitation

CLARID has certain limitations. It can occasionally select a suboptimal projection time step, t_e , or the total number of extraneous directions considered, n , as discussed in Section 3.4 and Section H in the Appendix. Calculating the singular vectors of the Jacobian of CDMs is computationally intensive. Whether the application of CLAReps can be effective on larger-scale problems, *e.g.*, ImageNet22K, remains a question.

6 Conclusion

We introduce Canonical LATent Representation Identifier (CLARID), a principled method to uncover the core categorical information encoded in pre-trained conditional diffusion models (CDMs). By removing extraneous directions from a sample’s latent code, CLARID produces *CLARep*, whose internal representation—Canonical Feature—distills the class-defining semantics of each category. Decoding CLAReps yields Canonical Samples that offer an interpretable and compact summary of the class. Quantitatively, Canonical Features form more compact and easily separable clusters in CDM feature space than the original inputs. Building on CLAReps, we have proposed ***CaDistill***, a diffusion-based feature distillation framework. The teacher CDM transfers core class semantics to the student only via CLAReps, which is equivalent to merely 10% of the original data, while the student is being trained on the full training set. The student achieves strong adversarial robustness and generalization on CIFAR-10 and ImageNet, focusing more on the true class signal instead of spurious background cues than the original model. Together, CLARID and ***CaDistill*** demonstrate that CDMs can be transformed from black-box generators into compact, interpretable teachers for robust representation learning.

Table 2: Results on the Backgrounds Challenge [79]. Higher is better. See Section K.5 in the Appendix for details.

Model	Original	BG-Same	BG-Rand	Only-FG
Vanilla	96.0	88.0	81.1	87.6
DiffAug [64]	96.1	87.5	80.3	87.4
DMDistill	96.3	88.0	80.6	84.5
CFGDistill	96.3	89.0	82.6	87.8
<i>CaDistill</i>	96.3	89.0	83.6	88.5

References

- [1] Maksym Andriushchenko, Francesco Croce, Nicolas Flammarion, and Matthias Hein. Square attack: a query-efficient black-box adversarial attack via random search. In *European Conference on Computer Vision*, pages 484–501. Springer, 2020.
- [2] Shekoofeh Azizi, Simon Kornblith, Chitwan Saharia, Mohammad Norouzi, and David J Fleet. Synthetic data from diffusion models improves imagenet classification. *Transactions on Machine Learning Research*.
- [3] Hritik Bansal and Aditya Grover. Leaving reality to imagination: Robust classification via generated datasets. In *ICLR 2023 Workshop on Trustworthy and Reliable Large-Scale Machine Learning Models*.
- [4] Fan Bao, Shen Nie, Kaiwen Xue, Yue Cao, Chongxuan Li, Hang Su, and Jun Zhu. All are worth words: A vit backbone for diffusion models. In *Proceedings of the IEEE/CVF Conference on Computer Vision and Pattern Recognition*, pages 22669–22679, 2023.
- [5] Dmitry Baranchuk, Andrey Voynov, Ivan Rubachev, Valentin Khrulkov, and Artem Babenko. Label-efficient semantic segmentation with diffusion models. In *International Conference on Learning Representations*, 2022.
- [6] Lucas Beyer, Olivier J Hénaff, Alexander Kolesnikov, Xiaohua Zhai, and Aäron van den Oord. Are we done with imagenet? *arXiv preprint arXiv:2006.07159*, 2020.
- [7] Nicholas Carlini and David Wagner. Towards evaluating the robustness of neural networks. In *2017 IEEE Symposium on Security and Privacy (SP)*, pages 39–57. IEEE, 2017.
- [8] Hila Chefer, Yuval Alaluf, Yael Vinker, Lior Wolf, and Daniel Cohen-Or. Attend-and-excite: Attention-based semantic guidance for text-to-image diffusion models. *ACM Transactions on Graphics (TOG)*, 42(4):1–10, 2023.
- [9] Siyi Chen, Huijie Zhang, Minzhe Guo, Yifu Lu, Peng Wang, and Qing Qu. Exploring low-dimensional subspace in diffusion models for controllable image editing. In *The Thirty-eighth Annual Conference on Neural Information Processing Systems*, 2024.
- [10] Xinlei Chen, Zhuang Liu, Saining Xie, and Kaiming He. Deconstructing denoising diffusion models for self-supervised learning. *arXiv preprint arXiv:2401.14404*, 2024.
- [11] Yixin Cheng, Grigorios Chrysos, Markos Georgopoulos, and Volkan Cevher. Multilinear operator networks. In *The Twelfth International Conference on Learning Representations*, 2023.
- [12] Edo Collins, Radhakrishna Achanta, and Sabine Susstrunk. Deep feature factorization for concept discovery. In *Proceedings of the European Conference on Computer Vision (ECCV)*, pages 336–352, 2018.
- [13] Francesco Croce and Matthias Hein. Reliable evaluation of adversarial robustness with an ensemble of diverse parameter-free attacks. In *International Conference on Machine Learning*, pages 2206–2216. PMLR, 2020.
- [14] Joel Dapello, Kohitij Kar, Martin Schrimpf, Robert Baldwin Geary, Michael Ferguson, David Daniel Cox, and James J DiCarlo. Aligning model and macaque inferior temporal cortex representations improves model-to-human behavioral alignment and adversarial robustness. In *The Eleventh International Conference on Learning Representations*, 2023.
- [15] Jia Deng, Wei Dong, Richard Socher, Li-Jia Li, Kai Li, and Li Fei-Fei. ImageNet: A large-scale hierarchical image database. In *2009 IEEE Conference on Computer Vision and Pattern Recognition*, pages 248–255. IEEE, 2009.
- [16] Prafulla Dhariwal and Alexander Nichol. Diffusion models beat gans on image synthesis. *Advances in Neural Information Processing Systems*, 34:8780–8794, 2021.

- [17] Josip Djolonga, Jessica Yung, Michael Tschannen, Rob Romijnders, Lucas Beyer, Alexander Kolesnikov, Joan Puigcerver, Matthias Minderer, Alexander D’Amour, Dan Moldovan, et al. On robustness and transferability of convolutional neural networks. In *Proceedings of the IEEE/CVF Conference on Computer Vision and Pattern Recognition*, pages 16458–16468, 2021.
- [18] Alexey Dosovitskiy, Lucas Beyer, Alexander Kolesnikov, Dirk Weissenborn, Xiaohua Zhai, Thomas Unterthiner, Mostafa Dehghani, Matthias Minderer, Georg Heigold, Sylvain Gelly, et al. An image is worth 16x16 words: Transformers for image recognition at scale. In *International Conference on Learning Representations*, 2020.
- [19] Arthur Douillard, Alexandre Ramé, Guillaume Couairon, and Matthieu Cord. DyTox: Transformers for continual learning with dynamic token expansion. In *Proceedings of the IEEE/CVF Conference on Computer Vision and Pattern Recognition*, pages 9285–9295, 2022.
- [20] Yunxiang Fu, Chaoqi Chen, Yu Qiao, and Yizhou Yu. Dreamda: Generative data augmentation with diffusion models. *arXiv preprint arXiv:2403.12803*, 2024.
- [21] Sven Gowal, Sylvestre-Alvise Rebuffi, Olivia Wiles, Florian Stimberg, Dan Andrei Calian, and Timothy A Mann. Improving robustness using generated data. *Advances in Neural Information Processing Systems*, 34:4218–4233, 2021.
- [22] René Haas, Inbar Huberman-Spiegelglas, Rotem Mulayoff, Stella Graßhof, Sami S Brandt, and Tomer Michaeli. Discovering interpretable directions in the semantic latent space of diffusion models. In *2024 IEEE 18th International Conference on Automatic Face and Gesture Recognition (FG)*, pages 1–9. IEEE, 2024.
- [23] Kaiming He, Xiangyu Zhang, Shaoqing Ren, and Jian Sun. Deep residual learning for image recognition. In *Proceedings of the IEEE Conference on Computer Vision and Pattern Recognition*, pages 770–778, 2016.
- [24] Ruifei He, Shuyang Sun, Xin Yu, Chuhui Xue, Wenqing Zhang, Philip Torr, Song Bai, and Xiaojuan Qi. Is synthetic data from generative models ready for image recognition? In *The Eleventh International Conference on Learning Representations*, 2023.
- [25] Dan Hendrycks and Thomas Dietterich. Benchmarking neural network robustness to common corruptions and perturbations. In *International Conference on Learning Representations*, 2018.
- [26] Amir Hertz, Ron Mokady, Jay Tenenbaum, Kfir Aberman, Yael Pritch, and Daniel Cohen-or. Prompt-to-prompt image editing with cross-attention control. In *The Eleventh International Conference on Learning Representations*.
- [27] Jonathan Ho and Tim Salimans. Classifier-free diffusion guidance. In *NeurIPS 2021 Workshop on Deep Generative Models and Downstream Applications*.
- [28] Jonathan Ho, Ajay Jain, and Pieter Abbeel. Denoising diffusion probabilistic models. *Advances in Neural Information Processing Systems*, 33:6840–6851, 2020.
- [29] Khawar Islam, Muhammad Zaigham Zaheer, Arif Mahmood, and Karthik Nandakumar. Dif-fusemix: Label-preserving data augmentation with diffusion models. In *Proceedings of the IEEE/CVF Conference on Computer Vision and Pattern Recognition*, pages 27621–27630, 2024.
- [30] Jaeseok Jeong, Mingi Kwon, and Youngjung Uh. Training-free content injection using h-space in diffusion models. In *Proceedings of the IEEE/CVF Winter Conference on Applications of Computer Vision*, pages 5151–5161, 2024.
- [31] Tero Karras, Miika Aittala, Timo Aila, and Samuli Laine. Elucidating the design space of diffusion-based generative models. *Advances in Neural Information Processing Systems*, 35: 26565–26577, 2022.
- [32] Tero Karras, Miika Aittala, Tuomas Kynkäänniemi, Jaakko Lehtinen, Timo Aila, and Samuli Laine. Guiding a diffusion model with a bad version of itself. *Advances in Neural Information Processing Systems*, 37:52996–53021, 2024.

- [33] Tero Karras, Miika Aittala, Jaakko Lehtinen, Janne Hellsten, Timo Aila, and Samuli Laine. Analyzing and improving the training dynamics of diffusion models. In *Proceedings of the IEEE/CVF Conference on Computer Vision and Pattern Recognition*, pages 24174–24184, 2024.
- [34] Prannay Khosla, Piotr Teterwak, Chen Wang, Aaron Sarna, Yonglong Tian, Phillip Isola, Aaron Maschinot, Ce Liu, and Dilip Krishnan. Supervised contrastive learning. *Advances in Neural Information Processing Systems*, 33:18661–18673, 2020.
- [35] Hoki Kim. Torchattacks: A pytorch repository for adversarial attacks. *arXiv preprint arXiv:2010.01950*, 2020.
- [36] Yunji Kim, Jiyoung Lee, Jin-Hwa Kim, Jung-Woo Ha, and Jun-Yan Zhu. Dense text-to-image generation with attention modulation. In *Proceedings of the IEEE/CVF International Conference on Computer Vision*, pages 7701–7711, 2023.
- [37] Diederik P Kingma and Jimmy Ba. Adam: A method for stochastic optimization. 2015.
- [38] Diederik P Kingma and Max Welling. Auto-encoding variational bayes. *arXiv preprint arXiv:1312.6114*, 2014.
- [39] Simon Kornblith, Mohammad Norouzi, Honglak Lee, and Geoffrey Hinton. Similarity of neural network representations revisited. In *International Conference on Machine Learning*, pages 3519–3529. PMLR, 2019.
- [40] Alex Krizhevsky, Geoffrey Hinton, et al. Learning multiple layers of features from tiny images. 2009.
- [41] Mingi Kwon, Jaeseok Jeong, and Youngjung Uh. Diffusion models already have a semantic latent space. In *International Conference on Learning Representations*, 2023.
- [42] Tuomas Kynkäänniemi, Miika Aittala, Tero Karras, Samuli Laine, Timo Aila, and Jaakko Lehtinen. Applying guidance in a limited interval improves sample and distribution quality in diffusion models. In *Conference on Neural Information Processing Systems*, 2024.
- [43] Alexander C Li, Mihir Prabhudesai, Shivam Duggal, Ellis Brown, and Deepak Pathak. Your diffusion model is secretly a zero-shot classifier. In *Proceedings of the IEEE/CVF International Conference on Computer Vision*, pages 2206–2217, 2023.
- [44] Daiqing Li, Huan Ling, Amlan Kar, David Acuna, Seung Wook Kim, Karsten Kreis, Antonio Torralba, and Sanja Fidler. Dreamteacher: Pretraining image backbones with deep generative models. In *Proceedings of the IEEE/CVF International Conference on Computer Vision*, pages 16698–16708, 2023.
- [45] Bingyan Liu, Chengyu Wang, Tingfeng Cao, Kui Jia, and Jun Huang. Towards understanding cross and self-attention in stable diffusion for text-guided image editing. In *Proceedings of the IEEE/CVF Conference on Computer Vision and Pattern Recognition*, pages 7817–7826, 2024.
- [46] Ze Liu, Yutong Lin, Yue Cao, Han Hu, Yixuan Wei, Zheng Zhang, Stephen Lin, and Baining Guo. Swin Transformer: Hierarchical vision transformer using shifted windows. In *Proceedings of the IEEE/CVF International Conference on Computer Vision*, pages 10012–10022, 2021.
- [47] Ze Liu, Han Hu, Yutong Lin, Zhuliang Yao, Zhenda Xie, Yixuan Wei, Jia Ning, Yue Cao, Zheng Zhang, Li Dong, et al. Swin Transformer v2: Scaling up capacity and resolution. In *Proceedings of the IEEE/CVF Conference on Computer Vision and Pattern Recognition*, pages 12009–12019, 2022.
- [48] Francesco Locatello, Stefan Bauer, Mario Lucic, Gunnar Raetsch, Sylvain Gelly, Bernhard Schölkopf, and Olivier Bachem. Challenging common assumptions in the unsupervised learning of disentangled representations. In *International Conference on Machine Learning*, pages 4114–4124. PMLR, 2019.
- [49] Aleksander Madry, Aleksandar Makelov, Ludwig Schmidt, Dimitris Tsipras, and Adrian Vladu. Towards deep learning models resistant to adversarial attacks. In *International Conference on Learning Representations*, 2018.

- [50] Leland McInnes, John Healy, Nathaniel Saul, and Lukas Großberger. Umap: Uniform manifold approximation and projection. *Journal of Open Source Software*, 3(29):861, 2018.
- [51] Benyuan Meng, Qianqian Xu, Zitai Wang, Xiaochun Cao, and Qingming Huang. Not all diffusion model activations have been evaluated as discriminative features. *Advances in Neural Information Processing Systems*, 37:55141–55177, 2024.
- [52] Soumik Mukhopadhyay, Matthew Gwilliam, Vatsal Agarwal, Namitha Padmanabhan, Archana Swaminathan, Srinidhi Hegde, Tianyi Zhou, and Abhinav Shrivastava. Diffusion models beat gans on image classification. *arXiv preprint arXiv:2307.08702*, 2023.
- [53] Soumik Mukhopadhyay, Matthew Gwilliam, Yosuke Yamaguchi, Vatsal Agarwal, Namitha Padmanabhan, Archana Swaminathan, Tianyi Zhou, Jun Ohya, and Abhinav Shrivastava. Do text-free diffusion models learn discriminative visual representations? In *European Conference on Computer Vision*, pages 253–272. Springer, 2024.
- [54] Wonpyo Park, Dongju Kim, Yan Lu, and Minsu Cho. Relational knowledge distillation. In *Proceedings of the IEEE/CVF Conference on Computer Vision and Pattern Recognition*, pages 3967–3976, 2019.
- [55] Yong-Hyun Park, Mingi Kwon, Jaewoong Choi, Junghyo Jo, and Youngjung Uh. Understanding the latent space of diffusion models through the lens of riemannian geometry. *Advances in Neural Information Processing Systems*, 36:24129–24142, 2023.
- [56] William Peebles and Saining Xie. Scalable diffusion models with transformers. In *Proceedings of the IEEE/CVF International Conference on Computer Vision*, pages 4195–4205, 2023.
- [57] Dustin Podell, Zion English, Kyle Lacey, Andreas Blattmann, Tim Dockhorn, Jonas Müller, Joe Penna, and Robin Rombach. Sdxl: Improving latent diffusion models for high-resolution image synthesis. In *International Conference on Learning Representations*, 2024.
- [58] Robin Rombach, Andreas Blattmann, Dominik Lorenz, Patrick Esser, and Björn Ommer. High-resolution image synthesis with latent diffusion models. In *Proceedings of the IEEE/CVF Conference on Computer Vision and Pattern Recognition*, pages 10684–10695, 2022.
- [59] Adriana Romero, Nicolas Ballas, Samira Ebrahimi Kahou, Antoine Chassang, Carlo Gatta, and Yoshua Bengio. Fitnets: Hints for thin deep nets. 2015.
- [60] Aninda Saha, Alina Bialkowski, and Sara Khalifa. Distilling representational similarity using centered kernel alignment (cka). In *Proceedings of the the 33rd British Machine Vision Conference (BMVC 2022)*. British Machine Vision Association, 2022.
- [61] Mert Bülent Sarıyıldız, Kartteek Alahari, Diane Larlus, and Yannis Kalantidis. Fake it till you make it: Learning transferable representations from synthetic imagenet clones. In *Proceedings of the IEEE/CVF Conference on Computer Vision and Pattern Recognition*, pages 8011–8021, 2023.
- [62] Christoph Schuhmann, Romain Beaumont, Richard Vencu, Cade Gordon, Ross Wightman, Mehdi Cherti, Theo Coombes, Aarush Katta, Clayton Mullis, Mitchell Wortsman, et al. Laion-5b: An open large-scale dataset for training next generation image-text models. *Advances in Neural Information Processing Systems*, 35:25278–25294, 2022.
- [63] Vikash Schwag, Saeed Mahloujifar, Tinashe Handina, Sihui Dai, Chong Xiang, Mung Chiang, and Prateek Mittal. Robust learning meets generative models: Can proxy distributions improve adversarial robustness? In *International Conference on Learning Representations*, 2022.
- [64] Chandramouli Shama Sastry, Sri Harsha Dumpala, and Sageev Oore. Diffaug: A diffuse-and-denoise augmentation for training robust classifiers. *Advances in Neural Information Processing Systems*, 37:20745–20785, 2024.
- [65] Jiaming Song, Chenlin Meng, and Stefano Ermon. Denoising diffusion implicit models. In *International Conference on Learning Representations*, 2021.

- [66] Yang Song, Jascha Sohl-Dickstein, Diederik P Kingma, Abhishek Kumar, Stefano Ermon, and Ben Poole. Score-based generative modeling through stochastic differential equations. In *International Conference on Learning Representations*, 2021.
- [67] Yue Song, Andy Keller, Nicu Sebe, and Max Welling. Latent traversals in generative models as potential flows. In *Proceedings of the 40th International Conference on Machine Learning*, pages 32288–32303, 2023.
- [68] Hugo Touvron, Matthieu Cord, Matthijs Douze, Francisco Massa, Alexandre Sablayrolles, and Hervé Jégou. Training data-efficient image transformers & distillation through attention. In *International Conference on Machine Learning*, pages 10347–10357. PMLR, 2021.
- [69] Hugo Touvron, Matthieu Cord, and Hervé Jégou. Deit iii: Revenge of the vit. In *European Conference on Computer Vision*, pages 516–533. Springer, 2022.
- [70] Brandon Trabucco, Kyle Doherty, Max A Gurinas, and Ruslan Salakhutdinov. Effective data augmentation with diffusion models. In *International Conference on Learning Representations*, 2024.
- [71] Ashish Vaswani, Noam Shazeer, Niki Parmar, Jakob Uszkoreit, Llion Jones, Aidan N Gomez, Łukasz Kaiser, and Illia Polosukhin. Attention is all you need. *Advances in Neural Information Processing Systems*, 30, 2017.
- [72] Peng Wang, Huijie Zhang, Zekai Zhang, Siyi Chen, Yi Ma, and Qing Qu. Diffusion model learns low-dimensional distributions via subspace clustering. In *NeurIPS 2024 Workshop on Mathematics of Modern Machine Learning*.
- [73] Zekai Wang, Tianyu Pang, Chao Du, Min Lin, Weiwei Liu, and Shuicheng Yan. Better diffusion models further improve adversarial training. In *International Conference on Machine Learning*, pages 36246–36263. PMLR, 2023.
- [74] Ross Wightman. Pytorch image models. <https://github.com/rwightman/pytorch-image-models>, 2019.
- [75] Ronald J Williams. Simple statistical gradient-following algorithms for connectionist reinforcement learning. *Machine Learning*, 8:229–256, 1992.
- [76] Sanghyun Woo, Shoubhik Debnath, Ronghang Hu, Xinlei Chen, Zhuang Liu, In So Kweon, and Saining Xie. Convnext v2: Co-designing and scaling convnets with masked autoencoders. In *Proceedings of the IEEE/CVF Conference on Computer Vision and Pattern Recognition*, pages 16133–16142, 2023.
- [77] Zhibiao Wu and Martha Palmer. Verbs semantics and lexical selection. In *Proceedings of the 32nd annual meeting on Association for Computational Linguistics*, pages 133–138, 1994.
- [78] Weilai Xiang, Hongyu Yang, Di Huang, and Yunhong Wang. Denoising diffusion autoencoders are unified self-supervised learners. In *Proceedings of the IEEE/CVF International Conference on Computer Vision*, pages 15802–15812, 2023.
- [79] Kai Yuanqing Xiao, Logan Engstrom, Andrew Ilyas, and Aleksander Madry. Noise or signal: The role of image backgrounds in object recognition. In *International Conference on Learning Representations*.
- [80] Jiarui Xu, Sifei Liu, Arash Vahdat, Wonmin Byeon, Xiaolong Wang, and Shalini De Mello. Open-vocabulary panoptic segmentation with text-to-image diffusion models. In *Proceedings of the IEEE/CVF Conference on Computer Vision and Pattern Recognition*, pages 2955–2966, 2023.
- [81] Yitao Xu, Tong Zhang, and Sabine Süsstrunk. Adanca: Neural cellular automata as adaptors for more robust vision transformer. In *The Thirty-Eighth Annual Conference on Neural Information Processing Systems*, 2024.
- [82] Shipeng Yan, Jiangwei Xie, and Xuming He. DER: Dynamically expandable representation for class incremental learning. In *Proceedings of the IEEE/CVF Conference on Computer Vision and Pattern Recognition*, pages 3014–3023, 2021.

- [83] Xingyi Yang and Xinchao Wang. Diffusion model as representation learner. In *Proceedings of the IEEE/CVF International Conference on Computer Vision*, pages 18938–18949, 2023.
- [84] Zhendong Yang, Zhe Li, Ailing Zeng, Zexian Li, Chun Yuan, and Yu Li. Vitkd: Feature-based knowledge distillation for vision transformers. In *Proceedings of the IEEE/CVF Conference on Computer Vision and Pattern Recognition*, pages 1379–1388, 2024.
- [85] Xufeng Yao, Yuechen ZHANG, Zuyao Chen, Jiaya Jia, and Bei Yu. Distill vision transformers to cnns via low-rank representation approximation. 2022.
- [86] Jiahui Yu, Zirui Wang, Vijay Vasudevan, Legg Yeung, Mojtaba Seyedhosseini, and Yonghui Wu. Coca: Contrastive captioners are image-text foundation models. *Transactions on Machine Learning Research*.
- [87] Tan Yu, Xu Li, Yunfeng Cai, Mingming Sun, and Ping Li. S2-mlp: Spatial-shift mlp architecture for vision. In *Proceedings of the IEEE/CVF Winter Conference on Applications of Computer Vision*, pages 297–306, 2022.
- [88] Sangdoo Yun, Dongyoon Han, Seong Joon Oh, Sanghyuk Chun, Junsuk Choe, and Youngjoon Yoo. Cutmix: Regularization strategy to train strong classifiers with localizable features. In *Proceedings of the IEEE/CVF International Conference on Computer Vision*, pages 6023–6032, 2019.
- [89] Sergey Zagoruyko and Nikos Komodakis. Paying more attention to attention: Improving the performance of convolutional neural networks via attention transfer. In *International Conference on Learning Representations*, 2017.
- [90] Hongyi Zhang, Moustapha Cisse, Yann N Dauphin, and David Lopez-Paz. Mixup: Beyond empirical risk minimization. In *International Conference on Learning Representations*, 2018.
- [91] Manyuan Zhang, Guanglu Song, Xiaoyu Shi, Yu Liu, and Hongsheng Li. Three things we need to know about transferring stable diffusion to visual dense prediction tasks. In *European Conference on Computer Vision*, pages 128–145. Springer, 2024.
- [92] Tong Zhang, Pan Ji, Mehrtash Harandi, Richard Hartley, and Ian Reid. Scalable deep k-subspace clustering. In *Computer Vision—ACCV 2018: 14th Asian Conference on Computer Vision, Perth, Australia, December 2–6, 2018, Revised Selected Papers, Part V 14*, pages 466–481. Springer, 2019.
- [93] Zijian Zhang, Zhou Zhao, and Zhijie Lin. Unsupervised representation learning from pre-trained diffusion probabilistic models. *Advances in Neural Information Processing Systems*, 35: 22117–22130, 2022.
- [94] Wenliang Zhao, Yongming Rao, Zuyan Liu, Benlin Liu, Jie Zhou, and Jiwen Lu. Unleashing text-to-image diffusion models for visual perception. In *Proceedings of the IEEE/CVF International Conference on Computer Vision*, pages 5729–5739, 2023.
- [95] Wenliang Zhao, Yongming Rao, Zuyan Liu, Benlin Liu, Jie Zhou, and Jiwen Lu. Unleashing text-to-image diffusion models for visual perception. In *Proceedings of the IEEE/CVF International Conference on Computer Vision*, pages 5729–5739, 2023.
- [96] Daquan Zhou, Zhiding Yu, Enze Xie, Chaowei Xiao, Animashree Anandkumar, Jiashi Feng, and Jose M Alvarez. Understanding the robustness in vision transformers. In *International Conference on Machine Learning*, pages 27378–27394. PMLR, 2022.
- [97] Zikai Zhou, Shitong Shao, Lichen Bai, Zhiqiang Xu, Bo Han, and Zeke Xie. Golden noise for diffusion models: A learning framework. *arXiv preprint arXiv:2411.09502*, 2024.
- [98] Zikai Zhou, Yunhang Shen, Shitong Shao, Linrui Gong, and Shaohui Lin. Rethinking centered kernel alignment in knowledge distillation. In *Proceedings of the Thirty-Third International Joint Conference on Artificial Intelligence*, pages 5680–5688, 2024.

Appendix: Table of Contents

A	An overview of the paper	18
B	Detailed Preliminaries	18
B.1	Denoising diffusion probabilistic model (DDPM)	18
B.2	Denoising diffusion implicit models (DDIM)	18
C	Random samples from <i>Tench</i> class generated by DiT	19
D	Class identity preservation when moving along extraneous directions	19
E	The layer index for Jacobian calculation	20
F	The generalization of CLARID	20
F.1	Fine-grained control of CLAReps with text conditioning	20
F.2	CLARID is compatible with the EDM sampler and UViT architecture	21
G	Details of the ImageNet20 experiment	21
G.1	Selecting the optimal layer and time step for feature extraction	22
G.2	On using NMI for measuring feature quality and the effectiveness of <i>CaDistill</i>	24
H	Choosing hyperparameters t_e and n for CLARID	24
H.1	Finding the optimal t_e	24
H.2	Choosing the total number of extraneous directions n for adaptively selecting k	24
H.2.1	Stable Diffusion 2.1	28
I	Details of the toy experiment	30
J	Training and evaluation details	31
K	More results on ImageNet	33
K.1	The performance of \mathcal{L}_{dist} alone in feature distillation	33
K.2	<i>CaDistill</i> is effective with different data augmentation strategies	33
K.3	<i>CaDistill</i> improves the student’s black-box adversarial robustness	34
K.4	Extracting class semantics using class tokens in vision transformer	34
K.5	Details of the Background Challenge	35
K.6	On the reproduction of RepFusion	35
K.7	Ablation studies	36
K.7.1	Number of CLAReps	36
K.7.2	The necessity of \mathcal{L}_{align} and \mathcal{L}_{cano} and their balance	36
K.7.3	The necessity of \mathcal{L}_{dist}	36
K.7.4	The weights of losses, λ_{cs} , λ_{dist} , λ_{cka}	36

K.7.5	The design of \mathcal{L}_{cano}	37
K.7.6	The magnitude of classifier-free guidance	38
K.8	Generalization of <i>CaDistill</i> to different student architectures	38
L	Discussion on the quantitative results	39
M	On more sophisticated feature distillation frameworks	39
N	More visual results	39
O	Broader Impact	45
P	License information	45
P.1	Datasets information and license	45
P.2	Model and code license	45

A An overview of the paper

We outline the paper in Figure 8.

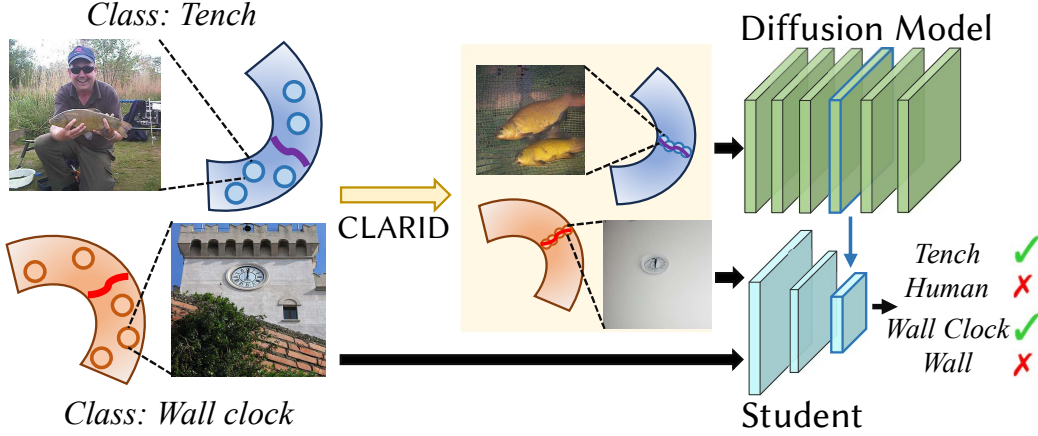


Figure 8: An overview of our paper. We identify the *CLAREps* via Canonical **L**atent **R**epresentation **I**dentifier (CLARID) inside conditional diffusion models (CDMs) as a compact family of latent codes that contain the core class information with minimal class-irrelevant signals. These prototypes lie on low-dimensional manifolds (red \sim and purple \sim tildes) within the latent space of CDMs. Leveraging the CLAREps, we design a diffusion-based **feature distillation** paradigm, improving the adversarial robustness and generalization of downstream models in image classification.

B Detailed Preliminaries

B.1 Denoising diffusion probabilistic model (DDPM)

DDPM [28] models the generation process as an inversion of a fixed forward Gaussian diffusion $q(\mathbf{x}_{1:T} | \mathbf{x}_0) := \prod_{t=1}^T q(\mathbf{x}_t | \mathbf{x}_{t-1})$. The forward kernel $q(\mathbf{x}_t | \mathbf{x}_{t-1})$ is described in Eq. 7.

$$q(\mathbf{x}_t | \mathbf{x}_{t-1}) = \mathcal{N}(\mathbf{x}_t; \sqrt{1 - \beta_t} \mathbf{x}_{t-1}, \beta_t \mathbf{I}) =: \mathcal{N}\left(\sqrt{\frac{\alpha_t}{\alpha_{t-1}}} \mathbf{x}_{t-1}, \left(1 - \frac{\alpha_t}{\alpha_{t-1}}\right) \mathbf{I}\right), \quad (7)$$

where $\{\beta_t\}_{t=1}^T$ is the variance schedule, $\alpha_t = \prod_{k=1}^t (1 - \beta_k)$. The inversion process is defined as $p_\theta(\mathbf{x}_{0:T}) := p(\mathbf{x}_T) \prod_{t=1}^T p_\theta(\mathbf{x}_{t-1} | \mathbf{x}_t)$, where $\mathbf{x}_T \sim \mathcal{N}(\mathbf{0}, \mathbf{I})$. θ denotes the parameter set of a trainable noise predictor \mathbf{f}_θ . A single reverse step is formalized in Eq. 8.

$$\mathbf{x}_{t-1} = \frac{1}{\sqrt{1 - \beta_t}} \left(\mathbf{x}_t - \frac{\beta_t}{\sqrt{\alpha_t}} \mathbf{f}_{\theta,t}(\mathbf{x}_t) \right) + \sqrt{\beta_t} \boldsymbol{\epsilon}_t, \quad \boldsymbol{\epsilon}_t \sim \mathcal{N}(\mathbf{0}, \mathbf{I}). \quad (8)$$

$\mathbf{f}_{\theta,t}$ means that the noise predictor receives t as a conditional input.

B.2 Denoising diffusion implicit models (DDIM)

DDIM [65] proposes a non-Markovian forward diffusion process, implying the parametrization described in Eq. 9.

$$q_\xi(\mathbf{x}_{t-1} | \mathbf{x}_t, \mathbf{x}_0) = \mathcal{N}\left(\sqrt{\alpha_{t-1}} \mathbf{x}_0 + \sqrt{1 - \alpha_{t-1} - \xi_t^2} \frac{\mathbf{x}_t - \sqrt{\alpha_t} \mathbf{x}_0}{\sqrt{1 - \alpha_t}}, \xi_t^2 \mathbf{I}\right), \quad (9)$$

where $\xi_t = \eta \sqrt{\frac{1 - \alpha_{t-1}}{1 - \alpha_t}} \sqrt{1 - \frac{\alpha_t}{\alpha_{t-1}}}$. The reverse step is described in Eq. 10.

$$\mathbf{x}_{t-1} = \left(\frac{\mathbf{x}_t - \sqrt{1 - \alpha_t} \mathbf{f}_\theta(\mathbf{x}_t)}{\sqrt{\alpha_t}} \right) + \sqrt{1 - \alpha_{t-1} - \xi_t^2} \mathbf{f}_\theta(\mathbf{x}_t) + \xi_t \boldsymbol{\epsilon}_t. \quad (10)$$



Figure 9: Random samples generated by DiT 256×256 [56] when conditioned on the *Tench* class (0th class in ImageNet).

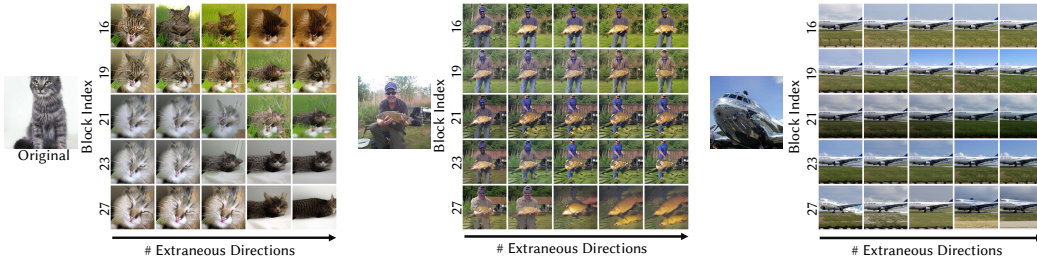


Figure 11: CLAReps when computing extraneous directions at different layers in a DiT [56]. We use $t_e = 0.8T$. Note that we do not use CFG after the extraneous directions projection, to present a more straightforward comparison between different layers. We choose $l = 27$, *i.e.* the last layer, to ensure an adequate change in the input.

DDIM and other parametrizations of the diffusion process [31, 33] can perform inversion on the input sample, retaining certain semantic information of it at $t = T$ [97].

C Random samples from *Tench* class generated by DiT

We sample random images using DiT-XL 256×256 [56] from the *Tench* class in ImageNet. We use a classifier-free guidance scale of 1.5, which is the one used in the original paper that achieves the best generation quality. The results are shown in Figure 9. Most images that we observe contain an angler.

D Class identity preservation when moving along extraneous directions

We show that the extraneous directions (Section 3.2) carry semantics that are not related to the class identity in Figure 10. We adopt the method proposed by Park et al. [55]. The editing focuses mostly on the background and preserves the class identity, as long as the movement does not orthogonalize the latent code and the editing direction. This phenomenon motivates our experiments.

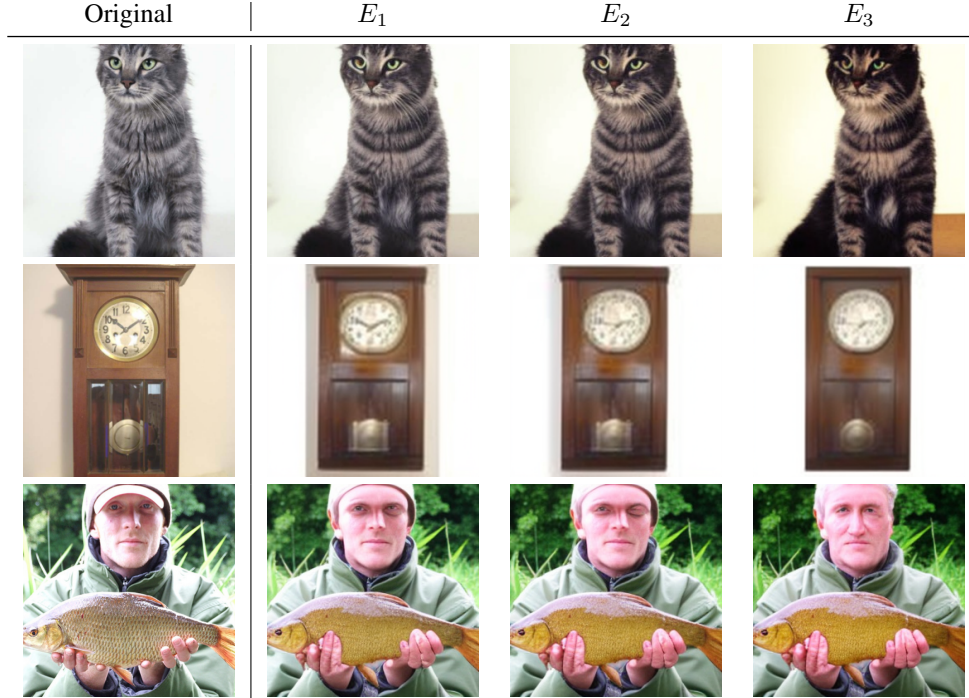


Figure 10: Moving along extraneous directions (Section 3.2) will alter the appearance of the image while preserving the class identity. E_i represents the editing strength.

E The layer index for Jacobian calculation

In Section 3.2, we treat the CDM as a feature extractor for calculating the Jacobian. We visualize the effect of selecting different l , *i.e.* the layer index for computing the Jacobian, in Figure 11. While in some cases different layers can yield similar effects, we choose the last layer, namely $l = 27$ (the minimum l is 0), to ensure an adequate change in the input, or the background can remain unchanged in certain cases.

For Stable Diffusion [58], we follow the practice in Park et al. [55] to select the layer index. Concretely, we extract the features after the middle block to ensure that the extraneous directions are semantically meaningful [30, 41]. We adopt the same strategy for all UNet-based CDMs, including the one used in our CIFAR10 experiments in Section 4.1 and the CDM in the EDM framework [31, 33].

F The generalization of CLARID

F.1 Fine-grained control of CLAReps with text conditioning

CLARID naturally extends to text-conditioning CDMs. Text-conditioning offers a more flexible control over where CLAReps lie than one-hot label conditioning. We show visual results in Figure 12 and 13. The used CDM, a Stable Diffusion 2.1 [58], successfully adapts to different text prompts on the same image, which is in line with previous findings [55]. In Figure 13, the CDM finds a CLARep that does not exist in the real world, but all the components in it are real, *e.g.* the water and the airplane. The results demonstrate that it is possible to perform a more fine-grained control over where CLAReps lie. We believe investigating the relationship between the CLAReps and the text conditioning on the same image can reveal the image understanding capability of CDMs, which we leave as a promising future direction.

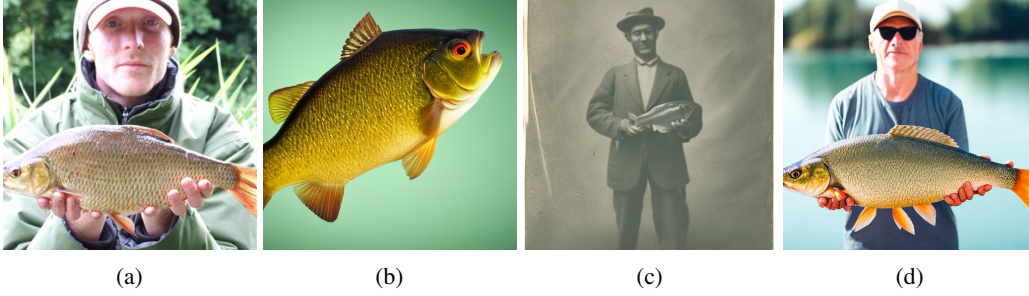


Figure 12: (a): The original image from the class *Tench*. (b): The CLARep obtained with prompt: *a photo of tench*. (c): The CLARep obtained with prompt: *a photo of a man holding a fish*. (d): An image generated with CFG using the same prompt as in (c), using the same starting noise as in (b) and (c).

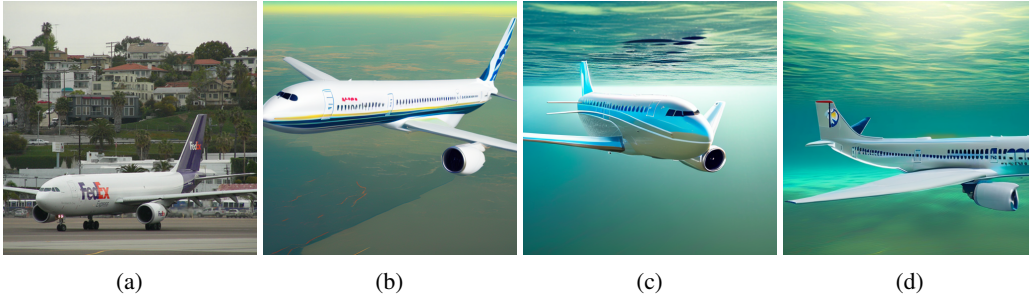


Figure 13: (a): The original image from the class *Airliner*. (b): The CLARep obtained with prompt: *a photo of airliner*. (c): The CLARep obtained with prompt: *an airplane flying under water*. (d): An image generated with CFG using the same prompt as in (c), using the same starting noise as in (b) and (c).

F.2 CLARID is compatible with the EDM sampler and UViT architecture

The main idea behind CLARID is to identify the latent vectors that carry non-discriminative information and render the latent code of a F_{inv} -inverted sample orthogonal to them. Such a formulation does not require any knowledge about the sampler or the architecture of the model, as long as the DM has enough capability to model the data distribution. Here, we demonstrate preliminary results on the generalization of CLARID. Specifically, we test the main idea behind CLARID on the EDM sampler [31, 33] with a UNet-based CDM, and a UViT [4] model using the same DDIM sampler as in the main paper. All CDMs are trained on ImageNet. We implement the inversion sampler of EDM. Here, we aim at showing the effectiveness of the identification of extraneous directions but not on the feature quality. Hence, we do not perform the same analysis as in Section 3.2.1. We present some visual results to demonstrate the intuitive summary of the categorical semantics, as shown in Figure 14 and 15. We believe investigating the relationship between the performance of the DM in generative tasks and it as teacher in *CaDistill* is promising, as previous works have found [73, 78], and leave it as a future work.

G Details of the ImageNet20 experiment

To develop the CLARID framework, we perform quantitative experiments on a 20-class subset of ImageNet [15]. This choice balances between computational costs and statistical significance. The indices of the 20 classes are: [15, 95, 146, 151, 211, 242, 281, 294, 385, 404, 407, 409, 440, 444, 499, 544, 579, 717, 765, 814]. The corresponding class names are: ['robin', 'jacamar', 'albatross', 'Chihuahua', 'vizsla', 'boxer', 'tabby', 'brown bear', 'Indian elephant', 'airliner', 'ambulance', 'analog clock', 'beer bottle', 'bicycle-built-for-two', 'cleaver', 'Dutch oven', 'grand piano', 'pickup', 'rocking chair', 'speedboat']. We plot the pair-wise Wu-Palmer (WUP) distances [77] between the selected classes in Figure 16. The selected classes can be similar or dissimilar to each other,

















	Class	Original	CLARID		Class	Original	CLARID
EDM [31, 33]	Tench			Wine Bottle			
							
	Airliner			Screen			
							

Figure 14: Preliminary results on Canonical Samples generated by the EDM framework [31, 33]. The left column is an EDM trained on ImageNet 64×64 , the right one is on ImageNet 512×512 . We implement the inversion sampler of EDM. It indicates that the main idea behind CLARID is also effective when facing inputs with different resolutions. Note that we do not use CFG or Autoguidance [32] to improve the visual quality, to provide a more straightforward insight into the effectiveness of CLARID on EDM.

		Class	Original	CLARID			Class	Original	CLARID
EDM [31, 33]	Robin					Goldfish			
	Jeep					Wall Clock			

Figure 15: Preliminary results on Canonical Samples generated by a ImageNet-256 UViT [4] using DDIM [65] sampler. It indicates that the main idea behind CLARID is effective on different architectures of CDMs. Note that we do not use CFG to improve the visual quality, to provide a more straightforward insight into the effectiveness of CLARID on UViT.

demonstrating certain structures. This is appropriate for analyzing the class separability in our case. We choose 50 images from the ImageNet20, building a 1000-sample dataset for the following analysis.

G.1 Selecting the optimal layer and time step for feature extraction

We choose an ImageNet 256×256 -pretrained DiT-XL [56] model for the quantitative analysis. We consider the outputs of all 28 ViT blocks in it. For the time step, we select $t_r = \{0.01, 0.05, 0.08, 0.1, 0.12, 0.15, 0.17, 0.2\}$. We perform K-means clustering on the feature map after average pooling, and compute the normalized mutual information between the cluster assignments and the ground truth class labels. The average pooling reduces noise in the feature map, making the cluster more accurate and compact. The results for different layers and time steps are shown in Figure 17, 18. Our conclusion on the time step for feature extraction is consistent with previous studies [52, 83] that adopt linear probing on the features for quantifying the feature quality, albeit with different DM architectures. Such a result provides **evidence on the validity of our metric, i.e. normalized mutual information.**

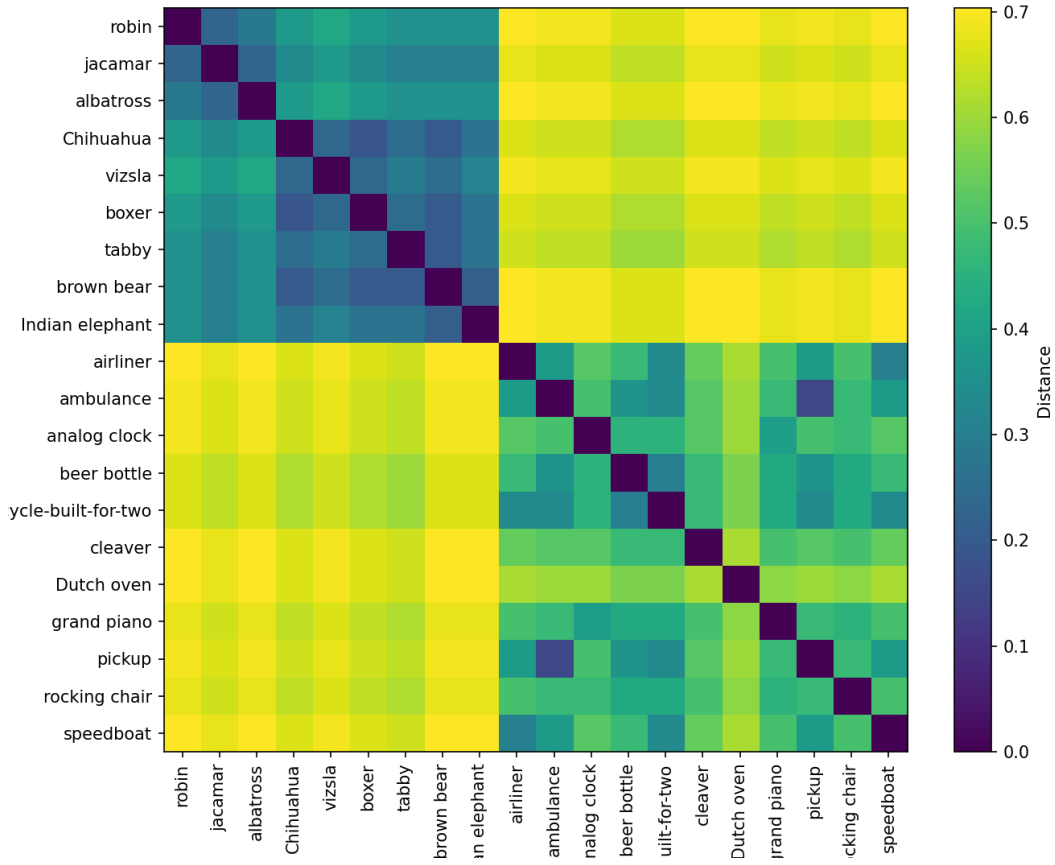


Figure 16: Wu-Palmer (WUP) distances (1.0-WUP similarity [77]) between the classes in ImageNet20. The class relationships are structured, hence appropriate for analyzing the class separability in our case.

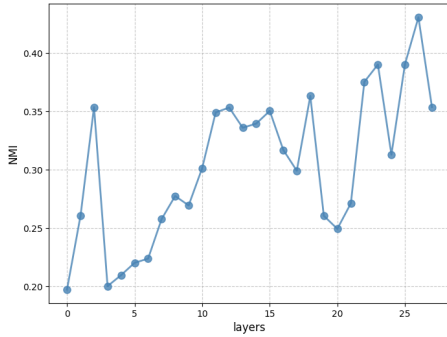


Figure 17: NMI v.s. layers on ImageNet20 in a DiT [56], fixing $t_r = 0.1T$. We choose the penultimate layer, *i.e.* the 27th layer (the figure has a 0-start index), in all our experiments.

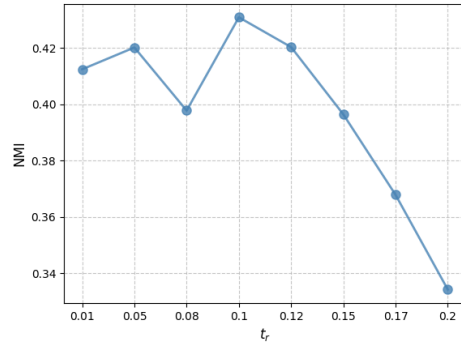


Figure 18: NMI v.s. feature extraction time step (t_r) on ImageNet20 using a DiT [56], fixing the layer index to be 27. We choose $t_r = 0.1T$ in all our experiments.

G.2 On using NMI for measuring feature quality and the effectiveness of *CaDistill*

While NMI is valid for self-evaluation of the feature quality within the CLARID framework, it is not valid for a direct comparison between the quality of features obtained via different methods, such as CFG. For example, when using CFG on the same 1000 samples after F_{inv} and extracting features at the same t_r as in CLARID, it can yield a higher NMI (0.6108 in CLARID v.s. 0.7808 with CFG magnitude being 4.0). Adopting CFG after performing extraneous direction projection can also improve the metric (0.7762 in CLARID with CFG being 3.0). However, NMI only examines the compactness and separability of each cluster, ignoring the low-dimensional manifold structure of the data. For example, a line-shaped manifold and a circle-shaped manifold can yield the same NMI, while they capture different characteristics of the data. In an extreme case where the features are constant for all samples belonging to the same class, the NMI will be 1.0, while the features are not meaningful in this case. **In other words, we do not want the student to just learn a "converging" prior on the features belonging to the same classes, but to learn actual class semantics.** This claim is validated in our extended ablation studies in Section K.7, where the student does not perform well when the CFG magnitude is high. These results undermine the notion that the student only mimics the CDM's label-conditioning embeddings: those embeddings behave as a trivial collapsing prior rather than conveying the encoded semantic structure. A promising future direction is to develop new feature quality metrics or adapt existing ones into CLARID that consider the structure of the data. This metric is also invalid on datasets with simple data structures, such as CIFAR10 [40]. The CDM features of the original samples are already perfectly separable and achieve an NMI of 1.0. However, as shown in Table 1 in the main paper, CLARID can still find more semantically meaningful samples than the original ones, and convey the knowledge to the student via *CaDistill*. While the simple structure of the data prevents the utilization of NMI, it is significantly easier to process than real image datasets. Either calculating the extraneous directions or training with *CaDistill* requires far less computational resources than large, real-image datasets such as ImageNet [15]. Therefore, we simply brute-force search the best hyperparameters in CLARID on CIFAR10. The hyperparameters on CIFAR10 are: $t_e = 0.8, n = 10, t_r = 0.13T$, layer = *up.0*. We also only use a 10% subset for obtaining CLAREps, as shown in Table 1.

H Choosing hyperparameters t_e and n for CLARID

H.1 Finding the optimal t_e

In Section 3.2, we decide t_e by finding the saturation point of classification accuracy on samples generated by our two-stage strategy. We use 3 classifiers and compute the average accuracy of them:

1. A ViT-Large pre-trained on ImageNet12K [15]. The input size is 224.
2. An ImageNet22k-pre-trained Swin V2 [47]. The input size is 256.
3. An ImageNet22k-pre-trained ConvNeXt V2 [76]. The input size is 384.

All model weights are downloaded from the PyTorch Image Model library (timm) [74]. The accuracy curve for DiT is shown in Figure 20. The maximum time step T is 1000 for both DiT [56] and Stable Diffusion [58]. We use DDIM as the sampler and set the total diffusion time step to 50. For each class, we generate 5 images. Hence $m = 5$ in Section 3.2. The prompt template for Stable Diffusion is: *a photo of <class name>*, where the class name is the WordNet name of each ImageNet class [15]. We identify $t_e = 800$ ($0.8T$) for DiT and $t_e = 1000$ (T) for Stable Diffusion. We provide visual comparisons between the images generated by selecting different t_e in Figure 21. Qualitatively, a small t_e might lead to insufficient changes in the input image, while a large t_e in DiT can fail to make the model aware of the class conditioning, resulting in less meaningful extraneous directions.

H.2 Choosing the total number of extraneous directions n for adaptively selecting k

Our key observation on selecting k , *i.e.* the number of extraneous directions to be projected, is that the effect caused by projecting extraneous directions is not smooth with varying k . That is, projecting one more extraneous directions can cause significant changes in the input. It is because extraneous directions are orthogonal to each other by design, hence there is no guarantee that their semantics are correlated. Importantly, projecting more extraneous directions does not necessarily mean a more

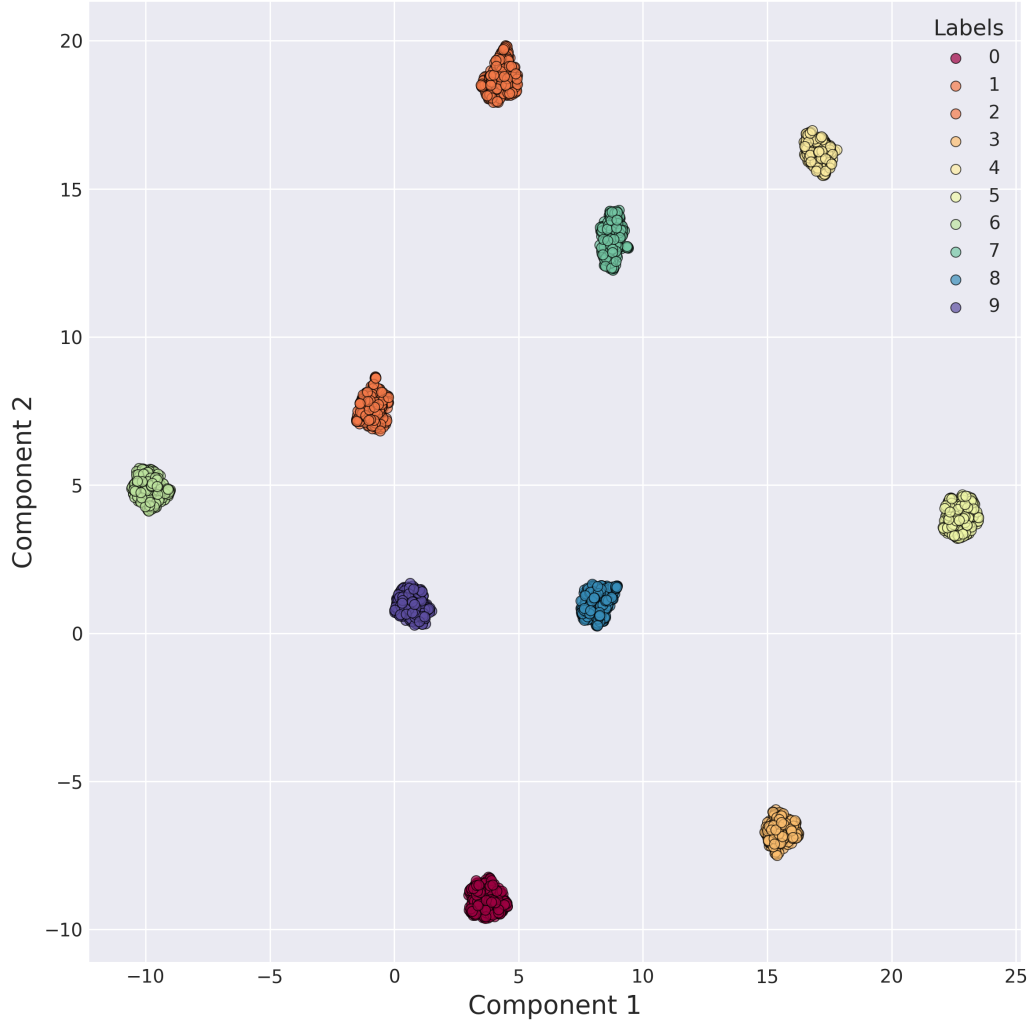


Figure 19: The CDM features of the original samples in CIFAR10 [40] are already separable and achieve an NMI of 1.0. However, CLARID is still effective in this case, as shown in Table 1.

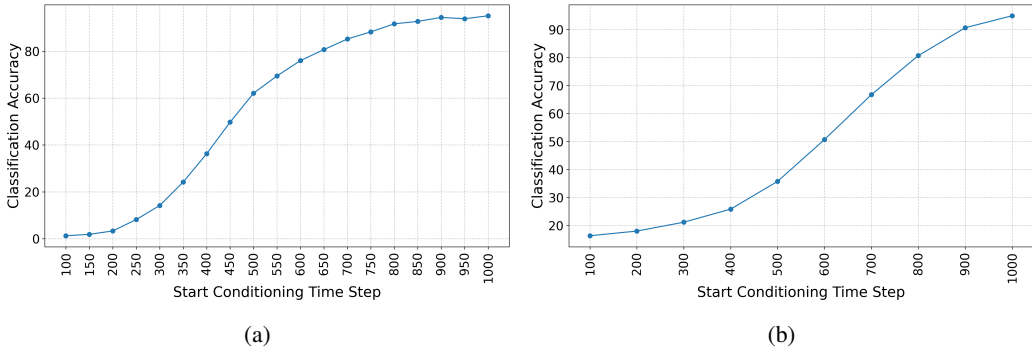
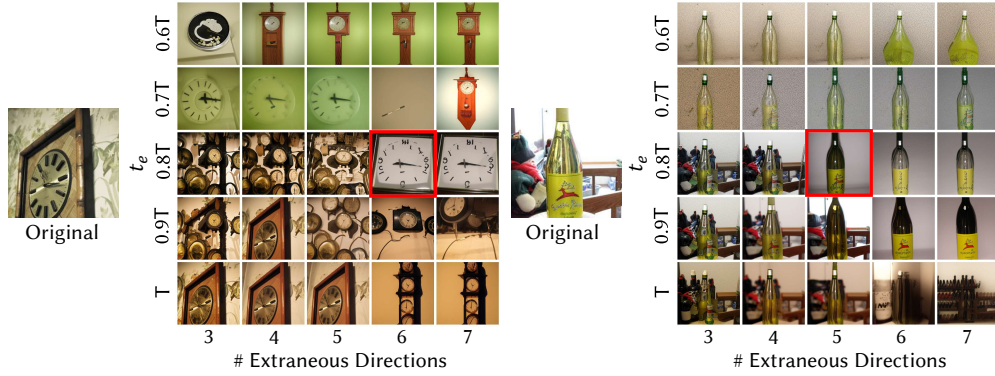
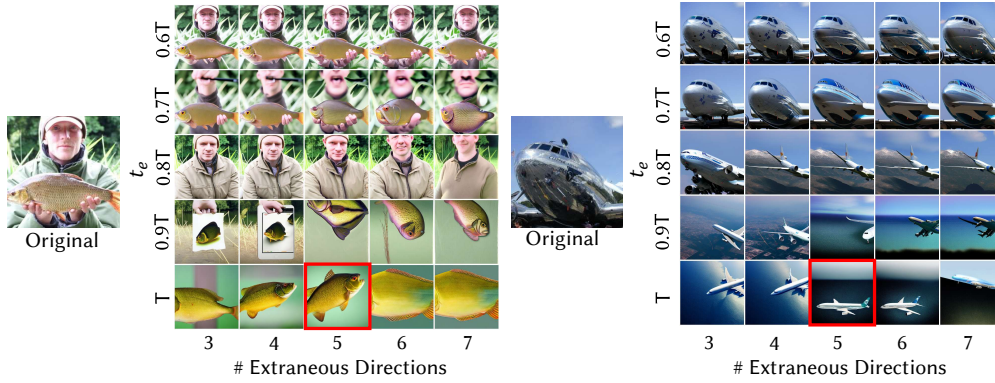


Figure 20: The classification accuracy on samples generated by the two-stage strategy in Section 3.2, using (a) DiT [56] and (b) Stable Diffusion [58]. The accuracy is averaged over 3 classifiers.

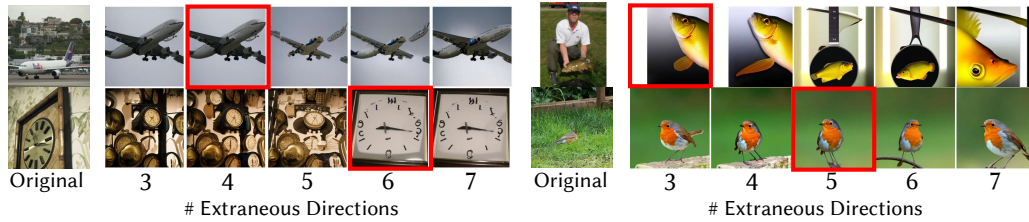


(a) Results of DiT.



(b) Results of Stable Diffusion.

Figure 21: Visual comparisons between the images generated by selecting different t_e and k in CLARID. Red boxes indicate the one automatically selected by our method.



(a) Results of DiT without CFG for a more straightforward comparison. (b) Results of Stable Diffusion with CFG magnitude being 7.5.

Figure 22: Visual comparisons between the images generated by selecting different k in CLARID. Red boxes indicate the one automatically selected by our method.

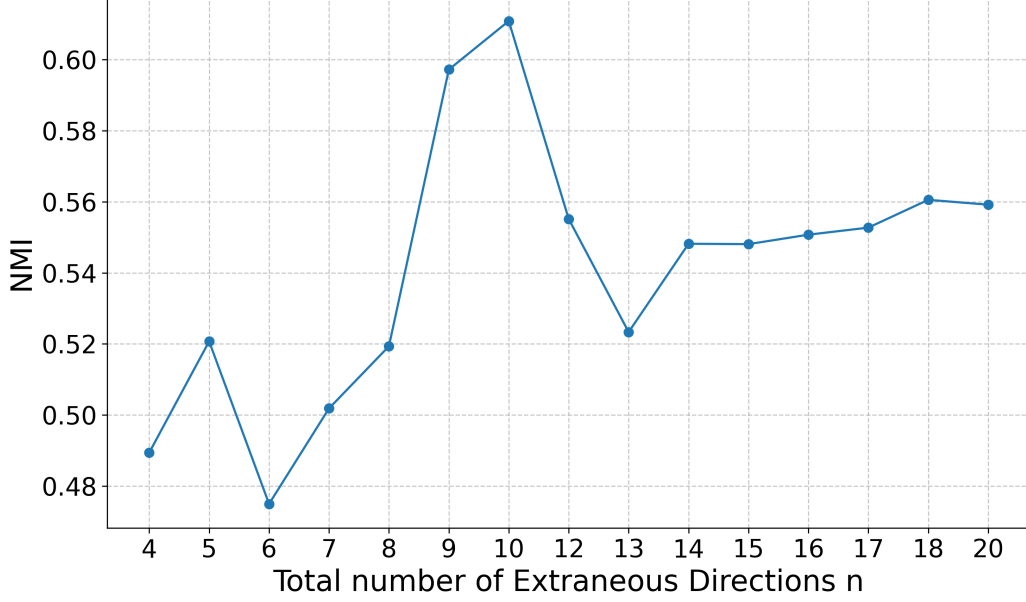


Figure 23: NMI on ImageNet20 v.s. total number of extraneous directions n on DiT. A large n can diminish the discriminative power of the input images, whereas a small one cannot change the inputs too much. Neither case is desired. Hence, we choose $n = 10$ for DiT in our experiment. Note that this is a self-evaluation within the CLARID framework, hence NMI is valid in this case.

separable set of Canonical Features. It can lead to a loss of the class-defining cues, as shown in the fish image in Figure 22b. We show the visual effects of selecting different k in Figure 21, 22. Our method CLARID selects k by adaptively choosing the elbow point on the explained variance ratio (EVR) sequence with total number of extraneous directions being n . The algorithm for finding the elbow point is presented in Algorithm 1.

Algorithm 1 Find Elbow via Knee Method(Sequence $S[0 \dots n - 1]$)

```

1:  $n \leftarrow |S|$ 
2:  $P_{\text{start}} \leftarrow (0, S[0])$ 
3:  $P_{\text{end}} \leftarrow (n - 1, S[n - 1])$ 
4:  $v \leftarrow P_{\text{end}} - P_{\text{start}}$ 
5:  $u \leftarrow v / \|v\|$ 
6: for  $i = 0$  to  $n - 1$  do
7:    $w \leftarrow (i, S[i]) - P_{\text{start}}$ 
8:    $\text{projLen} \leftarrow w \cdot u$ 
9:    $\text{projVec} \leftarrow \text{projLen} \times u$ 
10:   $\text{perpVec} \leftarrow w - \text{projVec}$ 
11:   $d[i] \leftarrow \|\text{perpVec}\|$ 
12: end for
13:  $k \leftarrow \arg \max_{0 \leq i < n} d[i]$ 
14: return  $k$ 

```

We show a quantitative comparison between different n in Figure 23 on ImageNet20. Too large n tends to select a larger k , leading to eliminating too many components in the input image and diminishing discriminative power. A small n will lead to a small k and cannot change the inputs too much. We select $n = 10$ for DiT, and $n = 11$ for SD in our experiment. Note that this n is tailored to specific CDMs. We plot the histogram of k when fixing $n = 10$ on 78000 images from ImageNet100, as we used in our experiments in Section K.7, in Figure 24. The selection process does not converge to a single k , supporting the effectiveness of our method. CLARID has certain fault

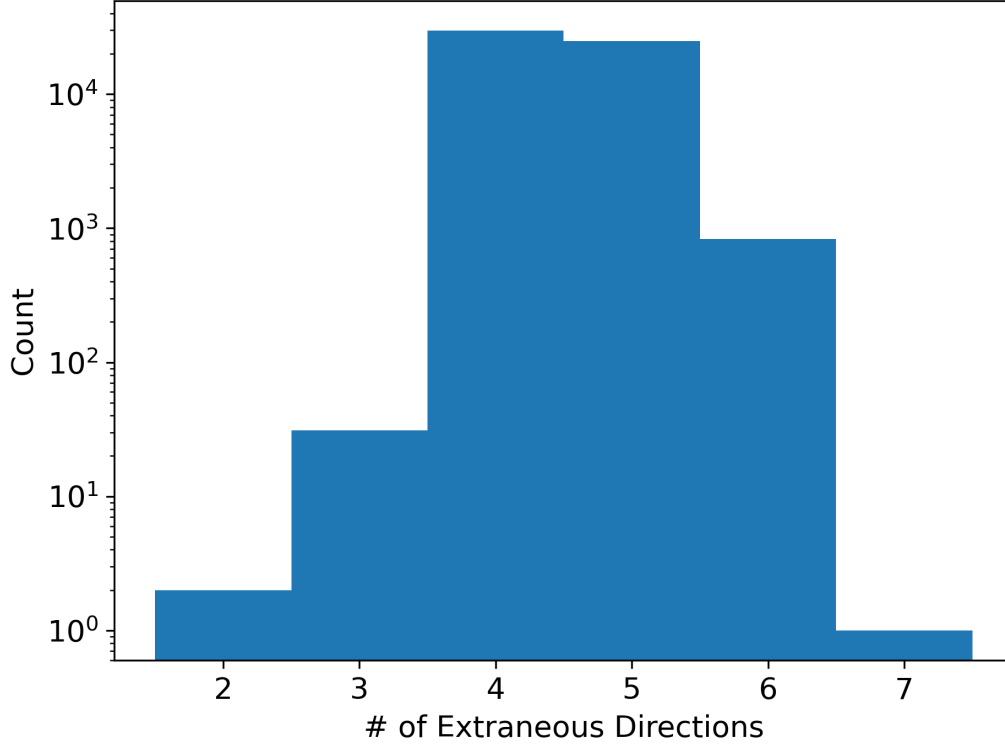


Figure 24: Histogram of k when fixing $n = 10$ on 78000 images from ImageNet100. We use this dataset in our experiments in Section K.7.

tolerance capacity, *i.e.* slightly changing the number of projected extraneous directions can still result in desired images. For example, in Figure 22, selecting $k = 3$ or $k = 4$ for the airplane image on DiT, or selecting $k = 3 \sim 7$ for the bird image on Stable Diffusion, can all result in desired outputs.

H.2.1 Stable Diffusion 2.1

We provide additional results on Stable Diffusion 2.1 model [58]. We first choose $t_r = 0.13T$ and the layer to be up_blocks.1, according to the results in Figure 25, 26. We then perform the same analysis as done in Section 3.2.1 in the main paper and Section H in the Appendix. Figure 27 shows the results. Observe that $t_e = T$, which is $t_e = 0.999$ in the figure, yields the best results when performing fixed- k projection. This validates our saturation-point-based t_e selection, as described in Section 3.2.1 in the main paper and Section H in the Appendix. Again, our CLARID produces the highest NMI among all other methods. In Figure 28, we show the different NMI results achieved by selecting different n for deciding k adaptively, and choose $n = 11$.

We identify some promising future directions. First, we fix t_e for all samples, which can be suboptimal on certain images. We only perform CLARID in a single time step instead of selecting multiple t_e . A series of projecting away extraneous directions has the potential of discarding more class-irrelevant information. Regarding the number of extraneous directions, we only perform experiments on cumulative projection, *i.e.* projecting away the top- k extraneous directions. A careful selection of the extraneous directions can contribute to better results. Due to the limits in computational resources, we leave them as future work. Occasionally, CLARID can also select suboptimal k , leading to artefacts in the generated images. We show failure cases for t_e and k in Figure 29, 30.

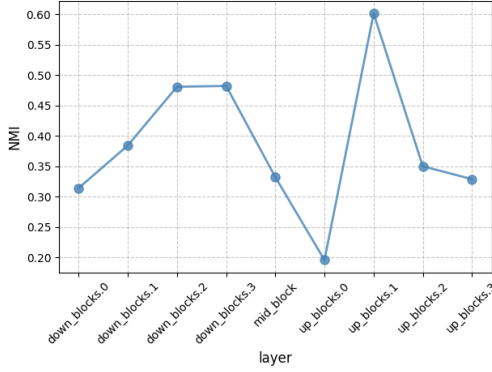


Figure 25: NMI v.s. layers on ImageNet20 in a Stable Diffusion 2.1 [58], fixing $t_r = 0.13T$. We choose the up_blocks.1 layer in all our experiments.

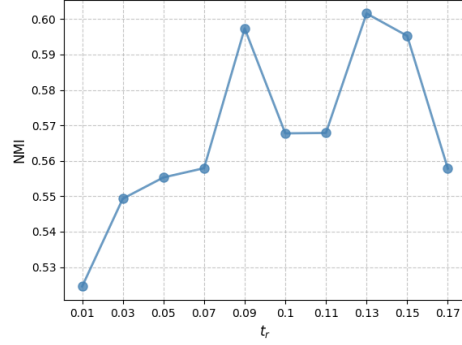


Figure 26: NMI v.s. feature extraction time step (t_r) on ImageNet20 using a Stable Diffusion 2.1 [58], fixing the layer index to be up_blocks.1.

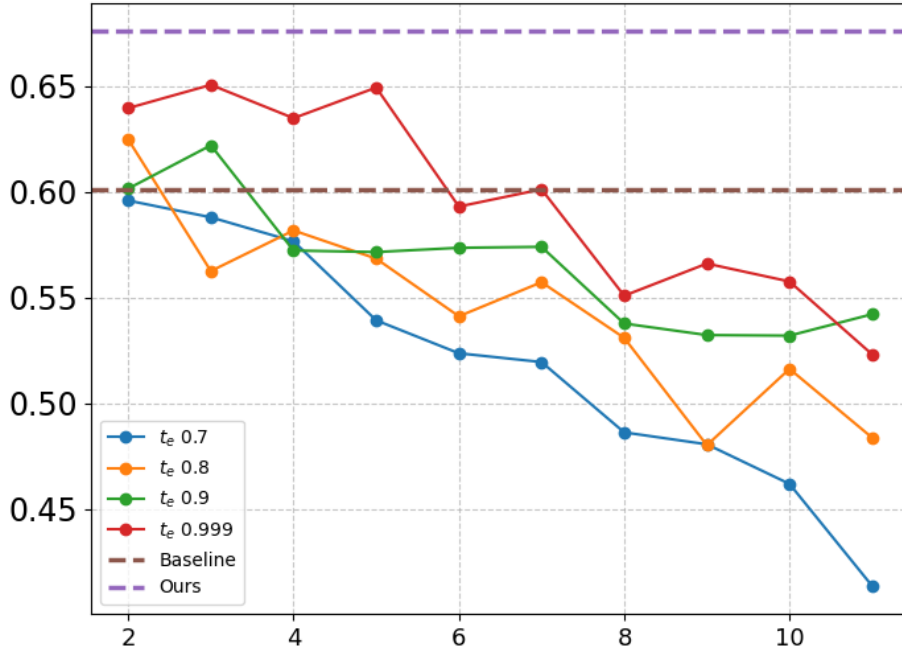


Figure 27: The normalized mutual information (NMI, higher is better) between cluster assignments of Stable Diffusion (SD) features using a Stable Diffusion 2.1 [58] and the ground truth labels. CLARID achieves the highest NMI. Baseline is the original SD features.

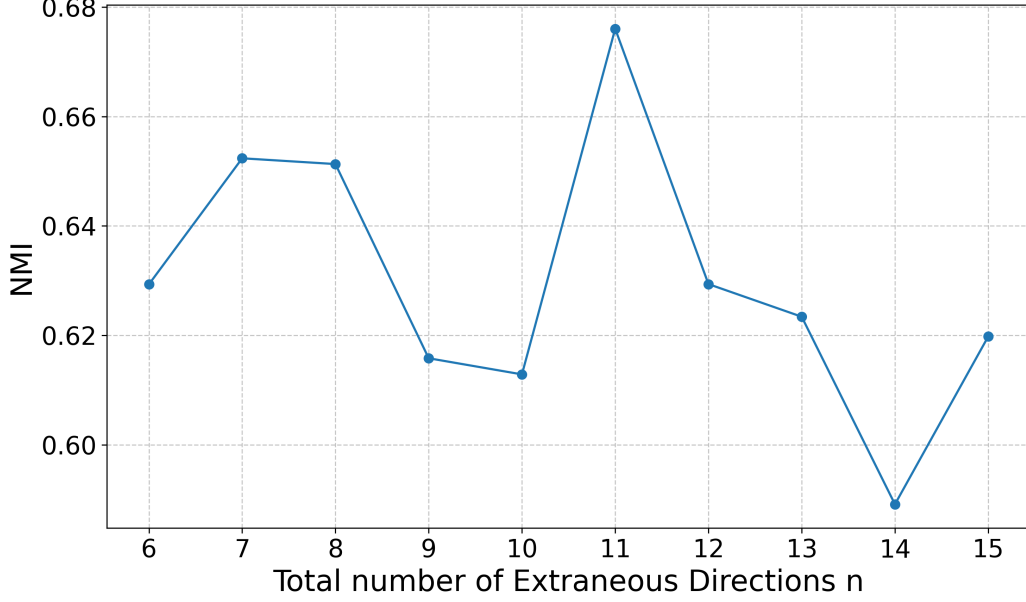


Figure 28: NMI on ImageNet20 v.s. total number of extraneous directions n on a Stable Diffusion 2.1 [58]. A large n can diminish the discriminative power of the input images, whereas a small one cannot change the inputs too much. Neither case is desired. Hence, we choose $n = 11$ for Stable Diffusion in our experiment. Note that this is a self-evaluation within the CLARID framework, hence NMI is valid in this case.

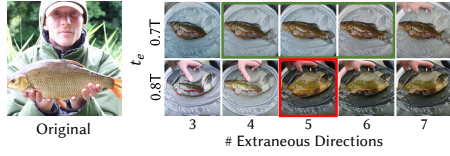


Figure 29: A Failure case of CLARID on selecting t_e . Green boxes are the optimal choice, qualitatively. Red boxes are the ones CLARID selects.



Figure 30: A Failure case of CLARID on selecting k when $n = 10$. Green boxes are the optimal choice, qualitatively. Red boxes are the ones CLARID selects.

I Details of the toy experiment

We adopt a hierarchical generative process described in Eq. 11 to generate 2D data points from two classes.

$$\begin{aligned}
 p(\mathbf{x}) &= p(y) p(\mathbf{x}_{\text{core}} | y) p(\mathbf{x}_{\text{var}} | \mathbf{x}_{\text{core}}), \\
 Y &\sim \text{Bernoulli}(\frac{1}{2}), \quad U \sim \mathcal{U}(-0.1, 0.1), \quad \boldsymbol{\varepsilon} = (\varepsilon_x, \varepsilon_y)^\top \sim \mathcal{N}(\mathbf{0}, 0.01 \mathbf{I}_2), \\
 \mathbf{s}(Y) &= \begin{cases} (0, 0)^\top, & Y = 0, \\ (4, 0)^\top, & Y = 1, \end{cases} \quad \mathbf{x}_{\text{core}} = (U, 0)^\top + \mathbf{s}(Y), \quad \mathbf{x}_{\text{var}} = \boldsymbol{\varepsilon}, \\
 \mathbf{x} &= \mathbf{x}_{\text{core}} + \mathbf{x}_{\text{var}} + (3|\varepsilon_y|, 0)^\top.
 \end{aligned} \tag{11}$$

In our toy model, we have two classes. We simulate the core class information by formulating the $p(\mathbf{x}_{\text{core}} | y)$, so that all data points sampled from $p(\mathbf{x}_{\text{core}} | \text{class1})$ lie on the line $L = \{(x_1, 0) | 3.9 \leq x_1 \leq 4.1\}$. We design the class-irrelevant variations to be $\boldsymbol{\varepsilon}$, sampled from a Gaussian distribution. We shift the x -axis value according to the y -axis variation to increase the complexity of the distribution. We design a simple 3-layer multilayer-perceptron-based (MLP-based) diffusion model to model this 2D distribution. We set the hidden dimensionality to 80, and the dimensionality for both label and time step is 16. We use sinusoidal embeddings for uniquely encoding the 1000 time steps [18]. We train the diffusion model using the standard DDPM loss [28]. The hyperparameters of training are

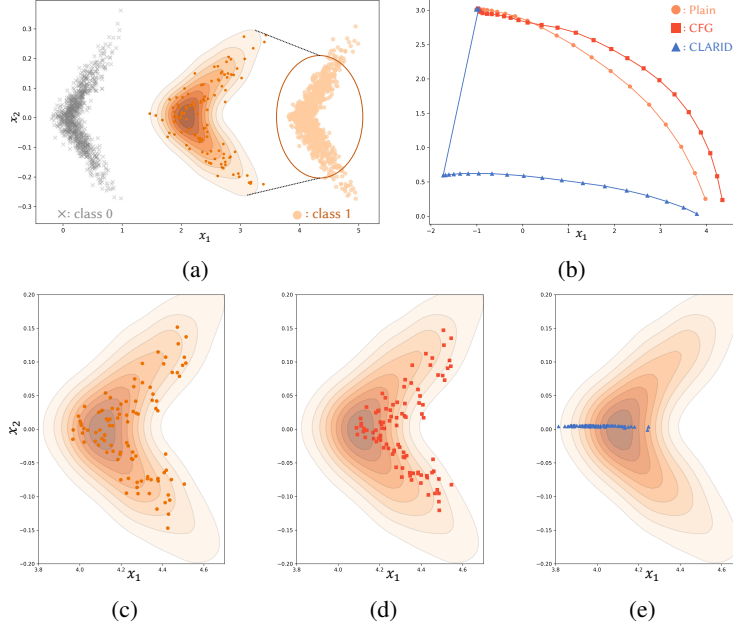


Figure 31: A toy example of CLARID. (a): The samples of class 0 and class 1; (b): Sampling trajectory of plain conditioning (Plain), classifier-free guidance (CFG), and CLARep (CLARID) starting from $F_{inv}([4.0, 0.2])$. CLARep (CLARID) orthogonalize the data latent code and class-irrelevant components encoded in the latent code in the CDM, yielding Canonical Samples; (c,d,e): The generated samples of Plain, CFG, and CLARID, respectively. CLAReps converge to a 1D manifold inside class 1, capturing the core class information.

Table 3: The hyperparameters used in our toy experiment in Section 3.3.

# data points	Epoch	Optimizer	Batch size	Learning rate	Weight decay	Label drop rate
1000	1000	Adam [37]	128	1e-3	0	0.1

given in Table 3. The resulting data points of CLARID, *i.e.* CLAReps, lie exactly on the line L . This is the reason why we claim that the underlying structure revealed by CLAReps corresponds to one of the true generative processes for the observed data.

J Training and evaluation details

We perform all the experiments using the PyTorch platform. We provide the training hyperparameters in Table 4. The temperature parameter τ in *CaDistill* is fixed to 0.1 in all cases, as in [34]. On CIFAR10, we use random crop (`torchvision.transforms.RandomCrop(32, padding=4)`) and random horizontal flip (`torchvision.transforms.RandomHorizontalFlip`) for data augmentation. Note that the SupCon [34] baseline uses a different data augmentation strategy and is trained for much longer epochs (1000). We follow the official code implementation (link) to reproduce this baseline on CIFAR10. On ImageNet and ImageNet100, we adopt the data augmentation used in Khosla et al. [34], to improve the generalization performance of the trained model so that the baselines have meaningful results on the used generalization benchmarks. For example, the ResNet50 trained with random resized crop and random horizontal flip, as in He et al. [23], will have 0% accuracy on ImageNet-A [17], while the baseline ResNet50 (Vanilla) in our experiments achieves 6.3%. The difference in data augmentation results in the performance difference on the ImageNet validation set between our baseline model and the one trained in He et al. [23]. However, we are not focusing on the clean performance in our settings. We use a single Nvidia A100 GPU for the CIFAR10 experiments, and four A100 GPUs for the ImageNet and ImageNet100 experiments. Training one model on CIFAR10 takes around 0.5 ~ 1 hour. Training on ImageNet takes around 40 hours for a model.

Table 4: The hyperparameters used in our experiments. We train a ResNet18 [23] on CIFAR10 and a ResNet50 on ImageNet. SGDM is SGD with momentum=0.9. *CaDistill* is effective with different training settings, as shown in Section K.2 and K.8.

\mathcal{D}	Epoch	Optimizer	Batch size	Learning rate	Weight decay	LR scheduler	LR decay rate
CIFAR10	200	SGDM	128	0.1	5e-4	Step 100,150	0.1
ImageNet100	100	SGDM	256	0.1	1e-4	Cosine	/
ImageNet	100	SGDM	512	0.1	1e-4	Cosine	/

Table 5: Hyperparameters in different adversarial attacks on CIFAR10.

	PGD [49]	CW [7]	APGD-DLR [13]	APGD-CE [13]
Max magnitude	2.0/255	/	2.0/255	2.0/255
Steps	5	5	5	5
Step size	0.5	/	/	/
κ	/	0.0	/	/
c	/	0.2	/	/
ρ	/	/	0.75	0.75
EOT	/	/	1	1

Our CaDistill involves the usage of CDM features, *i.e.*, Canonical Features. Instead of forwarding the CDM during training, which will lead to a large computational cost, we pre-compute the Canonical Features and load them during training, contributing to an efficient training pipeline. All Canonical Features are 1D vectors, which are the results of performing average pooling on the original feature map, as done in a previous work [83].

We examine the adversarial robustness of different student models using four adversarial attacks, PGD [49], CW [7], APGD-DLR [13], and APGD-CE [13]. The detailed settings are given in Table 5, 6, and 7 for CIFAR10, ImageNet, and ImageNet100 (AutoAttack), respectively. We choose PGD [49] since it is the most popular method for examining adversarial robustness [81]. Moreover, we want to examine whether the drawback of cross-entropy loss can lead to false robustness [13]. The step size in PGD can also largely affect the result. Hence, we choose the Auto-PGD family [13] to automatically decide the step size and incorporate the new Difference of Logits Ratio (DLR) loss, resulting in APGD-CE and APGD-DLR, respectively. We also want to include an optimization-based adversarial attack and thus select the CW [7] attack. The hyperparameters of different attacks are chosen to ensure a meaningful comparison between different models, avoiding the case in which all models have 0% accuracy after the attack. Our choices ensure a thorough test of the adversarial robustness in a white-box setting, revealing the multifacetedness of the adversarial robustness. Information about the generalization benchmarks is given in Section P.1.

Due to the limits in computational resources, we do not report error bars in our experiments. During testing, we find that different runs of adversarial attacks result in similar performance. We test each adversarial attack 3 times with different seeds and find that the resulting performance has standard deviations all smaller than 0.05.

Table 6: Hyperparameters in different adversarial attacks on ImageNet.

	PGD [49]	CW [7]	APGD-DLR [13]	APGD-CE [13]
Max magnitude	0.33/255	/	0.33/255	0.33/255
Steps	5	5	5	5
Step size	0.5	/	/	/
κ	/	0.0	/	/
c	/	0.1	/	/
ρ	/	/	0.75	0.75
EOT	/	/	1	1

Table 7: Hyperparameters of all attacks used in AutoAttack [13] in our ablation studies on ImageNet100.

	PGD [49]	CW [7]	APGD-DLR [13]	APGD-CE [13]
Max magnitude	0.5/255	/	0.5/255	0.5/255
Steps	5	10	5	5
Step size	0.5	/	/	/
κ	/	0.0	/	/
c	/	0.1	/	/
ρ	/	/	0.75	0.75
EOT	/	/	1	1

Table 8: Comparison between our CKA-based [39] \mathcal{L}_{dist} and other loss functions in diffusion-based feature distillation.

\mathcal{L}_{cano}	Clean	AutoAttack [13]
Vanilla [23]	86.5	15.9
FitNet [44, 59, 83]	86.7	16.4
AT [44, 83, 89]	86.6	16.3
RKD [54, 83]	86.2	16.4
Ours	87.3	18.8

K More results on ImageNet

K.1 The performance of \mathcal{L}_{dist} alone in feature distillation

In Section 4.1, we design a baseline experiment that distills the structure of the raw diffusion features into the representation space of the student network, which is based on \mathcal{L}_{dist} . Our design of \mathcal{L}_{dist} differs from all previous works on diffusion-based feature distillation. We use a CKA [39] metric for measuring the linear subspace alignment between the feature vectors of the student and the teacher. CKA is invariant to isotropic scaling as well as orthonormal transformations. Such an invariance lets us transfer the class-discriminative structure encoded in Canonical Features without over-constraining the student’s own feature basis. Previous works focus on using three classical feature distillation losses: (1) FitNet [44, 59, 83], which is the L2 distance between student features and the teacher’s; (2) Attention transfer (AT) [44, 83, 89], which distills the saliency structure of the activation map to the student; (3) Relational knowledge distillation (RKD) [54, 83], which aligns the relational representations of the samples between the teacher and the student. However, in our case, these loss functions do not significantly contribute to the student’s performance, as shown in Table 8. Note that in these experiments, the student features and the teacher ones are one-to-one matching to mimic the typical feature distillation framework, instead of the random strategy as we designed in *CaDistill*.

Our CKA-based [39] feature distillation loss outperforms all previous designs without introducing additional parameters during training. This is a novel loss function used in a diffusion-based feature distillation framework, inspired by previous works [14, 60, 98]. Performing knowledge transfer with the teacher and/or the student being a ViT is still an open question [84, 85], and can lead to a performance drop in the student. Our \mathcal{L}_{dist} , however, achieves good performance in the diffusion-based settings.

K.2 *CaDistill* is effective with different data augmentation strategies

We show that *CaDistill* is effective when the data augmentation strategy is different, demonstrating the generalization of the paradigm. Specifically, the training lasts 120 epochs, and the data augmentations are:

- `torchvision.transforms.RandomResizedCrop(224),`
- `torchvision.transforms.RandomHorizontalFlip(),`
- `torchvision.transforms.ColorJitter(0.3, 0.3, 0.3),`

Table 9: Quantitative comparisons between *CaDistill* and baselines on ImageNet [15] with a ResNet50 [23], using a different training setting (Section K.2) from the one in Section J. Higher is better.

Model	Data _{DM}	Clean	PGD [49]	CW [7]	APGD-DLR [13]	APGD-CE [13]	IM-C [25]	IM-A [17]	IM-ReaL [6]
Vanilla	/	76.6	17.3	13.5	18.8	17.7	40.6	3.4	83.3
<i>CaDistill</i>	10%	76.7	21.3	21.3	22.6	21.3	41.2	4.2	83.3

Table 10: Quantitative comparisons between *CaDistill*, and baselines on ImageNet [15] with a ResNet50 [23], on black-box adversarial robustness. Higher is better. **Red** is lower than the vanilla model. Data_{DM}: the portion of the subset on which the diffusion model serves as the teacher. DMDistill: Feature distillation by \mathcal{L}_{dist} on the whole dataset using a DiT model; CFGDistill: Using the framework of *CaDistill*, but replace CLAReps by samples with CFG from the CDM.

Model	Data _{DM}	Clean	Square [1]
Vanilla	/	75.9	23.5
DiffAug [64]	100%	76.0	20.7
DMDistill	100%	75.7	22.9
CFGDistill	10%	75.7	23.3
<i>CaDistill</i>	10%	75.9	25.6

The learning rate is 0.2, and the decay happens every 30 epochs with a decay rate of 0.1. The results are in Table 9. *CaDistill* yields a student that outperforms the vanilla model on all benchmarks, proving the effectiveness of our method in this case and implying its generalization capability.

K.3 *CaDistill* improves the student’s black-box adversarial robustness

In Table 1, we demonstrate that *CaDistill* improves the student’s white-box robustness. Here, we show that *CaDistill* improves the student performance when facing black-box adversarial attacks. Specifically, we test all models on ImageNet using the Square attack [1], which is a black-box adversarial attack algorithm. We use L_{inf} metric with attacking budget 4.0/255.0, and the query number is 1000. To reduce computational costs, we randomly select 2000 samples from ImageNet to perform the evaluation. The result is given in Table 10.

K.4 Extracting class semantics using class tokens in vision transformer

Our main claim on the application of CLAReps is that they distill the core class semantics of each category. Here, we investigate another mainstream approach to distill such information, which is the class token in vision transformer (ViT) [18, 68, 69]. The class token performs the attention operation [71] to all spatial tokens, collecting the discriminative signals inside the feature map for classification. We adopt a challenging baseline network, DeiT-III-Huge [69], which is a ViT model solely trained on ImageNet with the number of parameters (DeiT: 632.1M; DiT: 675M) and FLOPS (DeiT: 167.4G; DiT: 118.6G) matching the DiT [56] used in our experiments. It is challenging because the DeiT-III-Huge model is trained with advanced data augmentation techniques and performs well on ImageNet classification tasks [69], whereas DiT is trained with a plain horizontal flip augmentation and is not good at classification [43] (85.2 v.s. 77.5 Top-1 accuracy). We use our CKA-based \mathcal{L}_{dist} to align the representations of the student network to the class token in DeiT-III-Huge, termed DeiT_{dist}. All the settings are the same as used in Section 4.1 and J. The results are given in Table 11. Notably, the student trained with *CaDistill* outperforms the one trained with DeiT_{dist} in terms of clean accuracy and generalization. Achieving good performance in feature distillation between ViT and CNNs is still an open problem in the field [85]. Despite this, our experiments control the architecture (both teachers are ViTs), the number of parameters, and the FLOPS. Moreover, the DeiT_{dist} can yield a student that outperforms DMDistill in terms of all adversarial attack benchmarks, which demonstrates the effectiveness of the method and validity of our experiments. We believe investigating the difference between the mechanisms of how discriminative models and generative ones encode class information is an interesting future direction.

Table 11: Quantitative comparisons between ***CaDistill***, and baselines on ImageNet [15] with a ResNet50 [23]. Higher is better. **Red** is lower than the vanilla model. Data_{DM}: the portion of the subset on which the diffusion model serves as the teacher. DeiT_{dist}: Feature distillation by \mathcal{L}_{dist} on the whole dataset using the class token in an ImageNet-pretrained DeiT-III-Huge model [69]; DMDistill: Feature distillation by \mathcal{L}_{dist} on the whole dataset using a DiT model; CFGDistill: Using the framework of ***CaDistill***, but replace CLAReps by samples with CFG from the CDM.

Model	Data _{DM}	Clean	PGD [49]	CW [7]	APGD-DLR [13]	APGD-CE [13]	IM-C [25]	IM-A [17]	IM-Real [6]
Vanilla	/	75.9	15.6	13.7	17.2	16.7	45.9	6.3	82.8
DeiT _{dist} [69]	100%	75.1	19.7	18.4	20.8	20.3	45.2	5.4	82.5
DMDistill	100%	75.7	15.7	14.1	17.0	16.7	43.6	5.0	82.8
CFGDistill	10%	75.7	20.8	20.3	20.8	21.4	45.6	6.0	82.7
<i>CaDistill</i>	10%	75.9	21.9	21.7	22.5	22.3	46.1	6.7	83.1

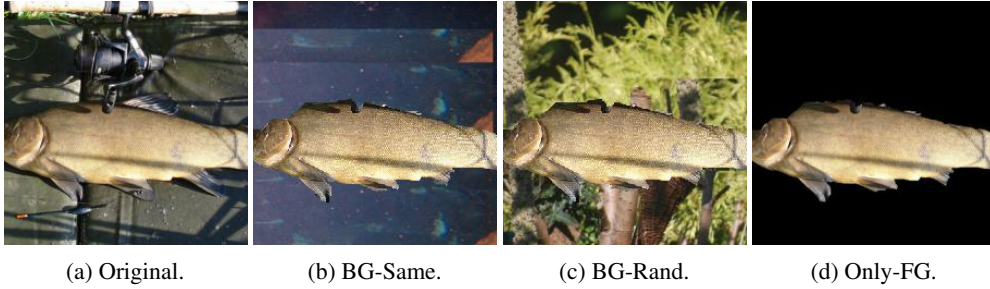


Figure 32: Samples from the Backgrounds Challenge [79]. (a) Original: The original image. (b) BG-Same: Put a random background from the same class onto the image. (c) BG-Rand: Put a random background from a different class onto the image. (d) Only-FG: Discard the background and make it black.

K.5 Details of the Background Challenge

In Section 4.1, we test the student model on the Backgrounds Challenge [79]. Figure 32 illustrates its three variants: BG-Same re-uses a single background per class; BG-Rand pairs each foreground with randomly chosen backgrounds from other classes; Only-FG removes the background entirely. These operations preserve the foreground object while removing background cues. Hence, the performance in this test quantifies a model’s ability to rely on true class signals rather than spurious background correlations.

As shown in Table 2, ***CaDistill*** achieves the highest accuracy across all splits. CFGDistill matches ***CaDistill*** on the Original and BG-Same sets, but ***CaDistill*** outperforms it on BG-Rand and Only-FG. This gap indicates that the student trained with CFGDistill still uses background information shared within each class; when those backgrounds are shuffled or removed, its accuracy declines. The evidence suggests that CFG introduces label-correlated yet non-essential background signals into the training data, whereas ***CaDistill*** suppresses those signals and encourages the student to focus on the foreground object.

K.6 On the reproduction of RepFusion

RepFusion [83] proposes a novel framework for diffusion-based feature distillation. It uses a neural network for adaptively selecting the time step of feature extraction from the teacher DM. This neural network is trained using the REINFORCE [75] algorithm, using the task performance as the reward. The task performance is the classification accuracy. In this case, the neural network is non-linear and can directly decode the label conditioning in the CDM to maximize the reward, leading to a failed training. Hence, we reproduce the method on an unconditional DM. Despite this, we provide a strong baseline using CDM, DMDistill, which uses a feature distillation loss that can outperform all the loss functions used in RepFusion, as shown in Section K.1.

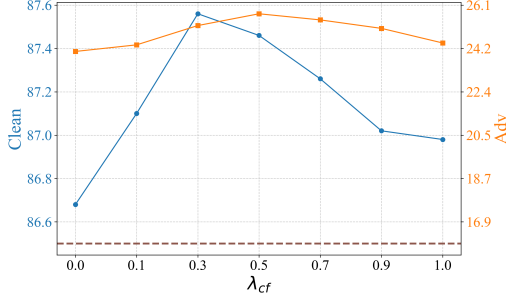


Figure 33: Ablation on λ_{cf} . An effective training requires a trade-off between \mathcal{L}_{align} and \mathcal{L}_{cano} , and necessitates both of them. We choose $\lambda_{cf} = 0.5$ to balance between the **Clean** accuracy and **robustness**. **Brown** is the baseline of both **Clean** and **Adv**.

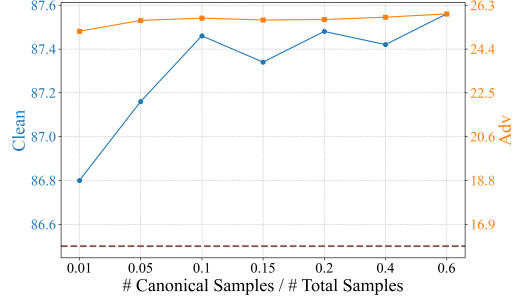


Figure 34: Ablation on the number of CLAReps. A small amount of CLAReps, *e.g.* 10%, is sufficient for achieving competitive performance. It implies the low-dimensionality property of the class manifolds inside CDMs, which is in line with previous findings [72].

K.7 Ablation studies

We conduct ablation studies on ImageNet100, a 100-class subset of ImageNet. Previous studies [11, 19, 81, 82, 87] have shown that ImageNet100 serves as a representative subset of ImageNet1K. Hence, we can obtain representative results for the self-evaluation of the model while efficiently using our computational resources. All the ablations are based on a ResNet50 [23] model. Note that we still use an ImageNet-pretrained DiT [56] as the teacher. We report the test accuracy on the ImageNet100 validation set as the clean accuracy (**Clean**), and the adversarial accuracy (**Adv**) under AutoAttack [13] that consists of PGD [49], CW [7], APGD-DLR [13], and APGD-CE [13].

K.7.1 Number of CLAReps

Figure 34 shows the student performance when trained with different numbers of CLAReps. Remarkably, training with as little as 10% of the available CLAReps already yields near-optimal performance. The result suggests that a small data subset is enough to capture the core semantics in CDMs, because those semantics lie on a low-dimensional manifold, which is consistent with earlier findings [72].

K.7.2 The necessity of \mathcal{L}_{align} and \mathcal{L}_{cano} and their balance

Our design includes on two complementary objectives: the alignment loss, \mathcal{L}_{align} , which pulls each sample towards CLAReps from its class, and the CLAREp separation loss, \mathcal{L}_{cano} , which drives the CLAReps of different classes apart. Figure 33 demonstrates the trade-off between the two. If \mathcal{L}_{align} is omitted ($\lambda_{cf} = 0$), samples remain distant from their canonical counterparts, preventing the student from learning the core semantics of each class. Conversely, dropping \mathcal{L}_{cano} ($\lambda_{cf} = 1$) can lead to CLAReps that collapse together, leaving the student unable to discriminate between categories. Therefore, the optimal choice requires a balance between them.

K.7.3 The necessity of \mathcal{L}_{dist}

The CDM transfers the core class features using Canonical Features via \mathcal{L}_{dist} . Without this loss, the student can fail to learn the encoded features of the Canonical Samples, which can negatively affect the student’s clean accuracy and adversarial robustness, as shown in Table 12.

K.7.4 The weights of losses, λ_{cs} , λ_{dist} , λ_{cka}

CaDistill involves 3 losses, λ_{cs} , λ_{dist} , λ_{cka} , each having its own weights. Here, we perform thorough ablation studies on λ_{cs} , λ_{dist} , λ_{cka} on ImageNet100. The results are given in Figure 35. We perform the ablation study on one loss function by fixing the other weights to their own optimal values. We empirically conclude this setting: $\lambda_{cs} = 0.4$, $\lambda_{dist} = 1.0$, $\lambda_{cka} = 0.5$, for all experiments on

Table 12: Quantitative comparisons between *CaDistill* and baselines on ImageNet [15] with a ResNet50 [23]. Vanilla: The original student network. Data_{DM}: the portion of the subset on which the diffusion model serves as the teacher. DMDistill: Feature distillation by \mathcal{L}_{dist} on the whole dataset; CFGDistill: Using the framework of *CaDistill*, but replace Canonical Samples by samples generated with CFG after F_{inv} , and use their corresponding features in the CDM. Higher is better. **Green** is lower than the vanilla model. Without \mathcal{L}_{dist} , the student cannot learn the teacher’s encoding of CLAReps, limiting the student’s adversarial robustness.

Model	Data _{DM}	Clean	PGD [49]	CW [7]	APGD-DLR [13]	APGD-CE [13]
Vanilla	/	75.9	15.6	13.7	17.2	16.7
DiffAug [64]	100%	76.0	15.9	13.1	17.2	17.0
DMDistill	100%	75.7	15.7	14.1	17.0	16.7
CFGDistill	10%	75.7	20.8	20.3	20.8	21.4
CaDistill	10%	75.9	21.9	21.7	22.5	22.3
No \mathcal{L}_{dist}	10%	75.6	20.3	19.3	20.5	21.9

ImageNet. For CIFAR10, we perform grid search over several parameter combinations and fix $\lambda_{cs} = 0.2, \lambda_{dist} = 0.25, \lambda_{cka} = 0.5$.

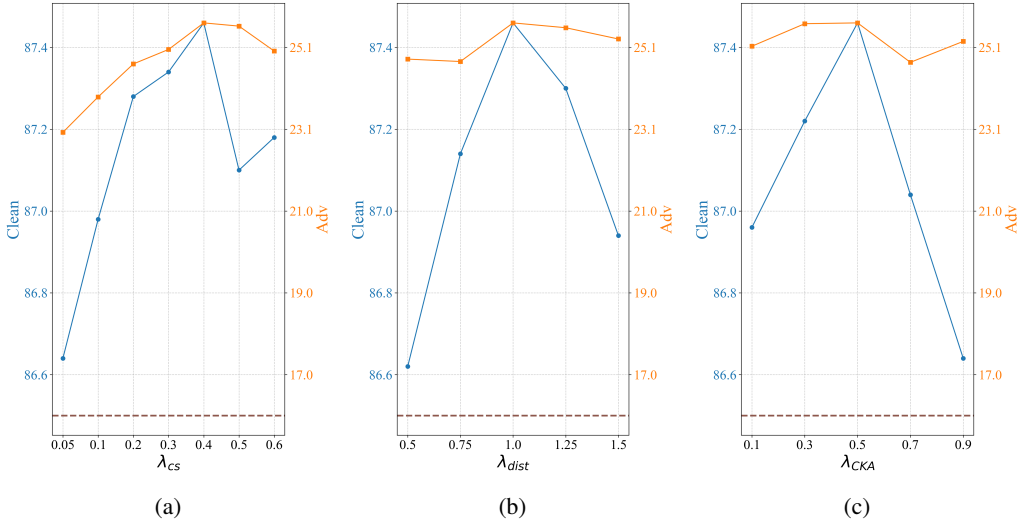


Figure 35: Ablation studies on $\lambda_{cs}, \lambda_{dist}, \lambda_{cka}$, introduced in Section 4. We select $\lambda_{cs} = 0.4, \lambda_{dist} = 1.0, \lambda_{cka} = 0.5$ in all of our experiments on ImageNet.

K.7.5 The design of \mathcal{L}_{cano}

We design \mathcal{L}_{align} and \mathcal{L}_{cano} to both have push-together and pull-away effects, inspired by Khosla et al. [34]. In Eq. (4), each Canonical Sample treats other Canonical Samples of the same class (excluding itself) as positive examples. If a class happens to contribute only a single Canonical Sample, no such positives exist. In that case, we optimize only the "pull-away" term—the denominator that separates the anchor from negatives in other classes, so the loss remains well-defined and informative. In this case, \mathcal{L}_{cano} becomes:

$$\mathcal{L}_{cano} = \frac{1}{b} \sum_{i=1}^b \log \sum_{k \neq i} \exp(\tilde{z}_i \cdot \tilde{z}_k / \tau). \quad (12)$$

We perform a simple ablation study on using cross-entropy for discriminating between CLAReps from different classes, using ImageNet100. The results are given in Table 13. Our design achieves better results in both clean accuracy and adversarial robustness, which is in line with the previous

Table 13: The ablation study on using cross-entropy as \mathcal{L}_{cano} . Our design in Eq. 4 achieves better results.

\mathcal{L}_{cano}	Clean	AutoAttack [13]
Vanilla [23]	86.5	15.9
Cross-entropy	86.8	25.3
Ours	87.5	25.7

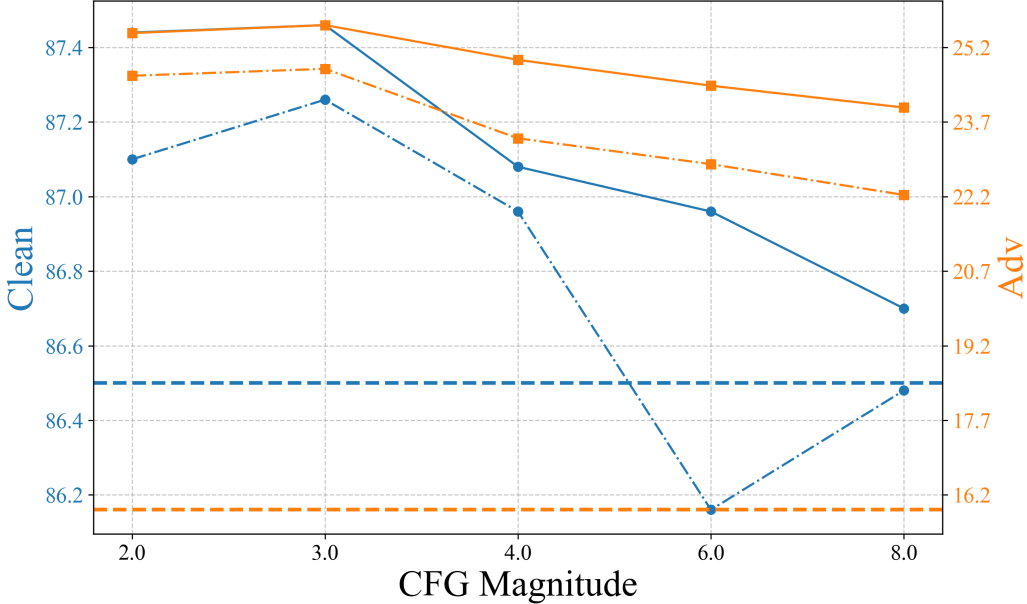


Figure 36: The ablation study on the magnitude of CFG used in our experiments on ImageNet. The student is trained with **CaDistill** (solid lines) and CFGDistill (dash-dot lines). The dashed lines are the baselines. Larger CFG magnitudes do not necessarily contribute to a better performance, indicating that our design in **CaDistill** is not simply a converging prior on the features (Section G.2).

claim [34]. In our case, CLAREps are far less than the original images and are easier to classify, which can cause overfitting issues when using cross-entropy and lead to suboptimal results.

K.7.6 The magnitude of classifier-free guidance

On ImageNet, we use CFG after projecting away the extraneous directions. We perform an ablation study on the CFG magnitude. The results are shown in Figure 36. Notably, larger CFG magnitudes do not correspond to better performance. An overly large CFG scale can even worsen student performance. This is because our **CaDistill** are not simply providing a converging prior over the student features, as discussed in Section G.2. We choose the magnitude to be 3 for both **CaDistill** and CFGDistill.

K.8 Generalization of **CaDistill** to different student architectures

We demonstrate that **CaDistill** is effective when the student is a transformer architecture. Specifically, we train a Swin-Tiny [46] model and a FAN-Tiny [96] model on ImageNet100. The result is given in Table 14. We train the networks using the same setting as described in Section J, except that we follow the timm data augmentation with Mixup [90] and CutMix [88], and we have a 5-epoch learning rate warm-up.

Table 14: Comparison between a vanilla Swin-Tiny [46] model, a FAN-Small [96] model, and the ones trained with *CaDistill*. Our method is effective with transformer students. It also proves that *CaDistill* is effective with modern data augmentation techniques such as Mixup [90] and CutMix [88].

Model	Clean	AutoAttack [13]
Swin-Tiny [46]	81.8	9.3
<i>CaDistill</i>	84.4	13.8
FAN-Tiny [96]	84.3	25.8
<i>CaDistill</i>	84.4	29.1

L Discussion on the quantitative results

Our proposed method, *CaDistill*, consistently improves the adversarial robustness and generalization ability of the student model. While the baseline methods can achieve better results on some benchmarks (*e.g.* the IM-C [25] test on DiffAug [64]), they can worsen the student’s performance on other benchmarks (Red marks). This phenomenon reveals the established observation: the multifacetedness of robustness. Despite this, *CaDistill* still consistently improves the student’s performance. The baseline methods that do not use our proposed feature distillation pipeline all necessitate access to the full dataset, while our methods achieve competitive performance with access only to 10% of the data.

The performance trends differ in CIFAR10 and ImageNet (Table 1). On CIFAR10, even if simply distilling the raw diffusion features to the student via DMDistill can contribute to the performance on all benchmarks, while on ImageNet, all the baseline methods can perform worse than the vanilla model in certain cases. We assume that two factors can lead to such a difference. The first is that CIFAR10 is a simpler dataset than ImageNet. Most images in CIFAR10 contain purely foreground objects, while the images in ImageNet are much noisier and harder to classify. The evidence is that CIFAR10 is a nearly solved dataset, as the classification accuracy approaches 100% [18], while the top models on ImageNet can achieve $\sim 90\%$ [86].

More importantly, we identify a critical difference in the CDM on CIFAR10 and on ImageNet. That is, ImageNet-trained CDMs are typically trained in a low-resolution latent space of a pre-trained variational autoencoder (VAE) [38, 58]. This low-resolution space loses detailed information compared to the pixel space, reducing the discriminative power. To validate, we train a ResNet50 [23] in this latent space for image classification, receiving the input as the VAE-encoded images. Notably, the clean accuracy drastically drops from 86.5 to 76.6. We assume that the missing discriminative information can negatively affect the performance of all feature distillation methods, because the diffusion features lie in the low-resolution latent space. Due to the limits on computational resources, we leave the investigation on pixel-space DM on ImageNet as a future direction.

M On more sophisticated feature distillation frameworks

In Section K.1, we demonstrate that our feature distillation loss outperforms the ones used in existing diffusion-based feature distillation frameworks. In this experiment, we use a single-layer distillation framework. That is, the alignment between the student and the teacher only happens at one layer, respectively. We do not consider more sophisticated feature distillation frameworks such as multi-layer alignments [44, 84] due to limited computational resources. We believe investigating the combinations between *CaDistill* and different feature distillation frameworks is a promising future direction.

N More visual results

We provide more visualizations of CLAReps using Canonical Samples obtained from the DiT [56] used in our *CaDistill* experiments on ImageNet [15], in Figure 37, 38, 39, 40, 41. All the classes are from ImageNet.

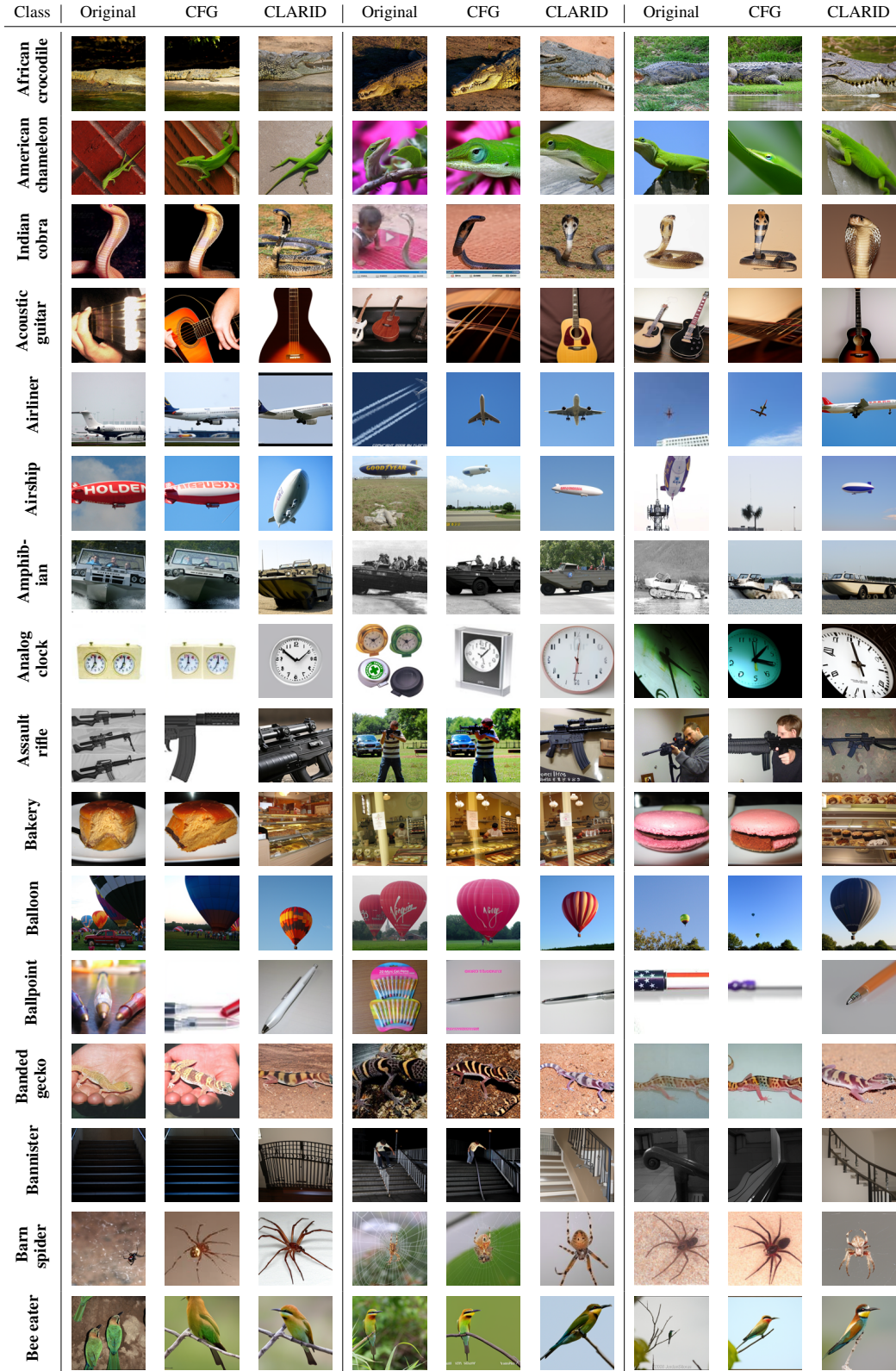


Figure 37: Visualizations of CLAREps using Canonical Samples obtained from the DiT [56] used in our *CaDistill* experiments on ImageNet.



Figure 38: Visualizations of CLAReps using Canonical Samples obtained from the DiT [56] used in our *CaDistill* experiments on ImageNet.

Class	Original	CFG	CLARID	Original	CFG	CLARID	Original	CFG	CLARID
American lobster									
Chihuahua									
English foxhound									
Maltese dog									
Cleaver									
Conch									
Dugong									
Isopod									
Jellyfish									
King crab									
Limpkin									
Otterhound									
Oystercatcher									
Red backed sandpiper									
Sea anemone									
Snail									

Figure 39: Visualizations of CLAReps using Canonical Samples obtained from the DiT [56] used in our *CaDistill* experiments on ImageNet.

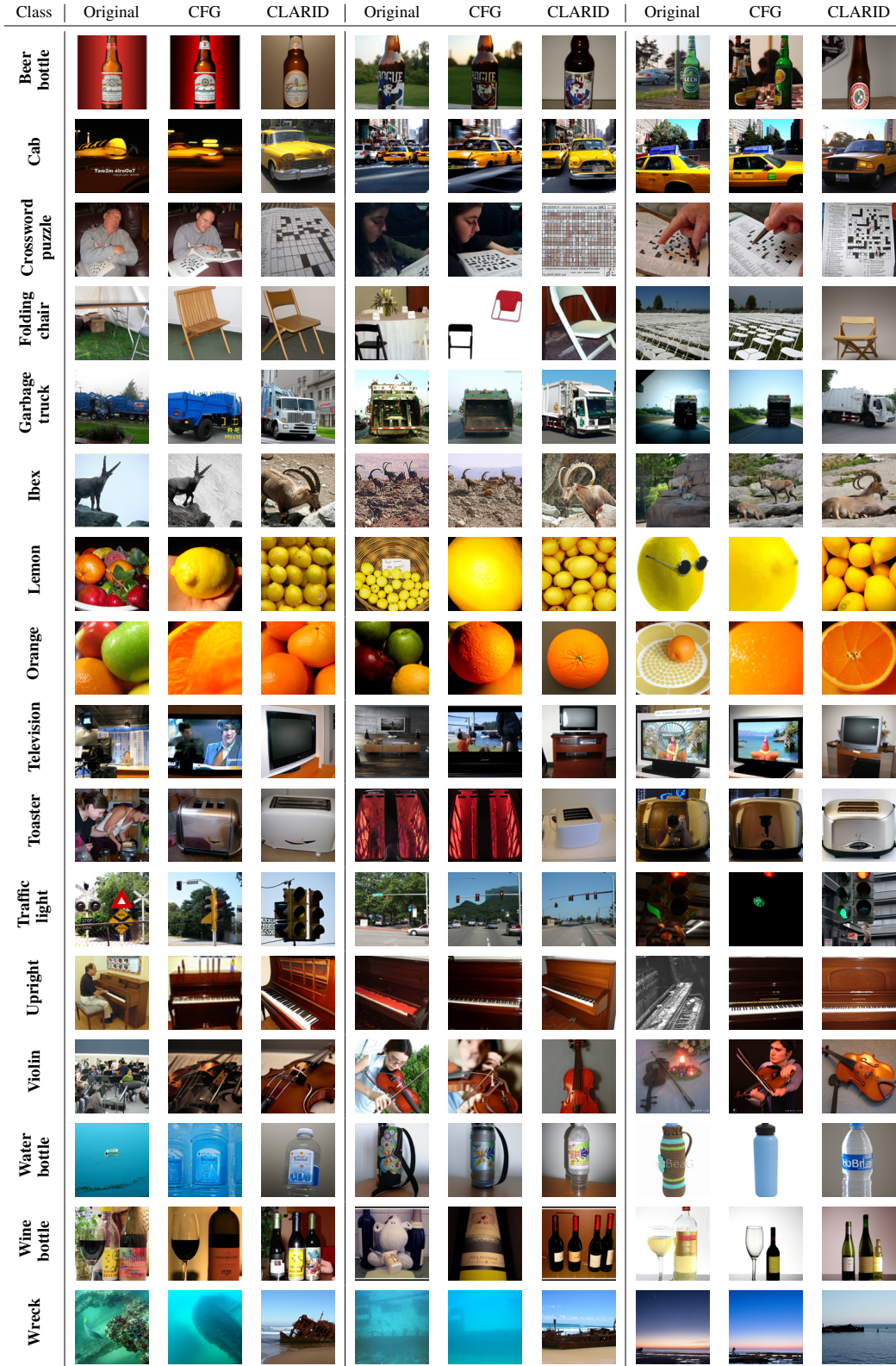


Figure 40: Visualizations of CLAReps using Canonical Samples obtained from the DiT [56] used in our *CaDistill* experiments on ImageNet.

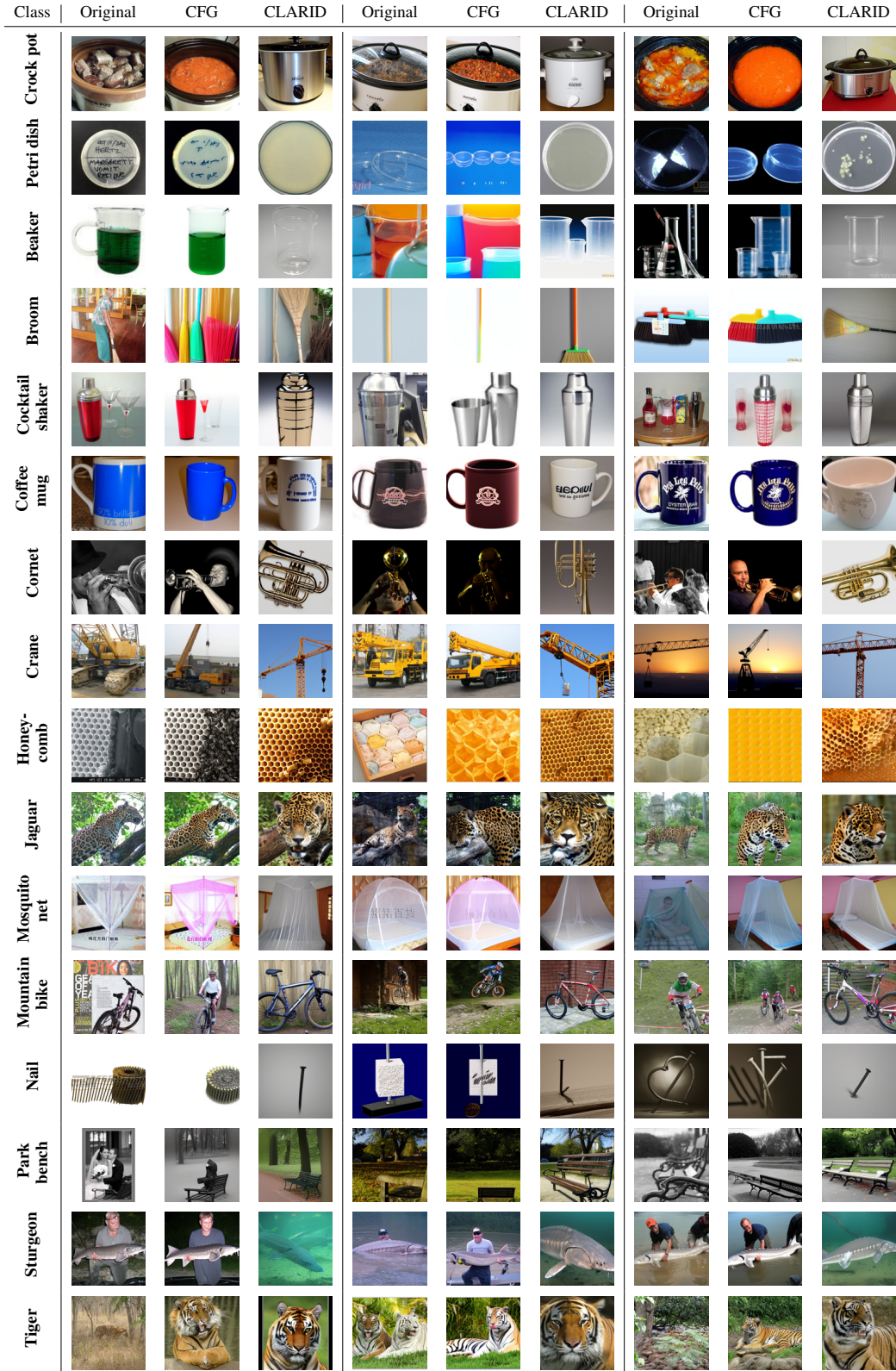


Figure 41: Visualizations of CLAReps using Canonical Samples obtained from the DiT [56] used in our *CaDistill* experiments on ImageNet.

O Broader Impact

CLARID introduces a new avenue into the field of DM research, focusing on interpreting the discriminative signals inside CDMs rather than directly probing the raw feature space. Our findings advance the interpretability of CDMs, contributing to safer usage of them. The application of CLAReps challenges the common assumption that the usage of DMs for discriminative tasks necessitates a large amount of data, providing new directions in diffusion-based feature distillation. The image generators used in our experiments may sometimes contain wrong information. That said, we are not focusing on generating high-fidelity images or improving the synthesizing quality.

P License information

P.1 Datasets information and license

- ImageNet1K [15]. This dataset contains 1.28M training images and 50000 images for validation. We report the top1 accuracy on the 50000 validation images. License: Custom (research, non-commercial).
- ImageNet-C [25]. This dataset contains 15 types of 2D image corruption types that are generated by different algorithms. Higher accuracy on this dataset indicates a more robust model against corrupted images. License: CC BY 4.0.
- ImageNet-A [17]. This dataset contains naturally existing adversarial examples that can drastically decrease the accuracy of ImageNet1K-trained CNNs. It is a 200-class subset of the ImageNet1K dataset. License: MIT license.
- ImageNet Reassessed Labels (ImageNet-ReaL) [6]: This is a dataset with 50000 reassessed labels of the ImageNet validation set, aiming at testing the in-distribution generalization ability of a classifier. License: Apache 2.0 License.
- CIFAR10-C [25]. This dataset contains 15 types of 2D image corruption types that are generated by different algorithms. Higher accuracy on this dataset indicates a more robust model against corrupted images. License: CC BY 4.0.

P.2 Model and code license

- Code for adversarial attacks [35]: MIT License.
- PyTorch Image Model [74]: Apache 2.0 License.
- Diffusion Transformer (DiT) [56]: Attribution-NonCommercial 4.0 International.
- Stable Diffusion 2.1 [58]: CreativeML Open RAIL++-M License.
- EDM2 [33]: Creative Commons BY-NC-SA 4.0 license.
- Supervised Contrastive Learning [34]: BSD 2-Clause License.
- Swin [46]: MIT License.
- FAN [96]: Nvidia Source Code License-NC.